2003-12

Broadband counterwound spiral antenna for subsurface radar applications

Lim, Teck Yong

Monterey, California. Naval Postgraduate School

NAVAL POSTGRADUATE SCHOOL

MONTEREY, CALIFORNIA

THESIS

BROADBAND COUNTER-WOUND SPIRAL ANTENNA FOR SUBSURFACE RADAR APPLICATIONS

by

Lim Teck Yong

December 2003

Thesis Advisor:	David Jenn
Second Reader:	Jeffrey B. Knorr

Approved for public release, distribution is unlimited

THIS PAGE INTENTIONALLY LEFT BLANK

REPORT DOCUMENTATION PAGE			Form Approved OMB No. 0704-0188
Public reporting burden for this collection of information is estimated to average 1 hour per response, including the time for reviewing instruction, searching existing data sources, gathering and maintaining the data needed, and completing and reviewing the collection of information. Send comments regarding this burden estimate or any other aspect of this collection of information, including suggestions for reducing this burden, to Washington headquarters Services, Directorate for Information Operations and Reports, 1215 Jefferson Davis Highway, Suite 1204, Arlington, VA 22202-4302, and to the Office of Management and Budget, Paperwork Reduction Project (0704-0188) Washington DC 20503.			
1. AGENCY USE ONLY *(Leave blank)*	**2. REPORT DATE** December 2003	**3. REPORT TYPE AND DATES COVERED** Master's Thesis	
4. TITLE AND SUBTITLE: Broadband Counter-wound Spiral Antenna for Subsurface Radar Applications			**5. FUNDING NUMBERS**
6. AUTHOR(S) Lim Teck Yong			
7. PERFORMING ORGANIZATION NAME(S) AND ADDRESS(ES) Naval Postgraduate School Monterey, CA 93943-5000			**8. PERFORMING ORGANIZATION REPORT NUMBER**
9. SPONSORING /MONITORING AGENCY NAME(S) AND ADDRESS(ES) N/A			**10. SPONSORING/MONITORING AGENCY REPORT NUMBER**
11. SUPPLEMENTARY NOTES The views expressed in this thesis are those of the author and do not reflect the official policy or position of the Department of Defense or the U.S. Government.			
12a. DISTRIBUTION / AVAILABILITY STATEMENT Approved for public release, distribution is unlimited			**12b. DISTRIBUTION CODE**

13. ABSTRACT ***(maximum 200 words)***

Subsurface radar, also known as ground-penetrating radar, is increasingly being used for the detection and location of buried objects such as mines and structures that are found within the upper regions of the earth's surface. The thesis gives a review of the work done to date in this area, laying emphasis on the possible antenna designs to match the range of intended applications. An overall design strategy is outlined, together with a more detailed treatment of the ground-penetrating radar subsystems and topics which are relevant to effective subsurface radar operation. These include the dielectric properties of earth materials, the choice of frequency of operation, as well as the design and construction of suitable antennas.

Finally, a new antenna structure called the counter-wound spiral antenna, which is suitable for subsurface radar applications, is examined. The counter-wound spiral antenna has a broad bandwidth and a linear polarization with a controllable plane of polarization from a planar geometry. It has an electronically steerable plane of polarization. This unique property offers a reduction in antenna polarization loss and allows the extraction of maximum information from the target scattered echo.

14. SUBJECT TERMS Subsurface Radar, Ground-Penetrating Radar System, Frequency Independence antenna, Spiral Antennas, ground dielectric properties.			**15. NUMBER OF PAGES** 95
			16. PRICE CODE
17. SECURITY CLASSIFICATION OF REPORT Unclassified	**18. SECURITY CLASSIFICATION OF THIS PAGE** Unclassified	**19. SECURITY CLASSIFICATION OF ABSTRACT** Unclassified	**20. LIMITATION OF ABSTRACT** UL

NSN 7540-01-280-5500 Standard Form 298 (Rev. 2-89)
Prescribed by ANSI Std. 239-18

THIS PAGE INTENTIONALLY LEFT BLANK

Approved for public release, distribution is unlimited

BROADBAND COUNTERWOUND SPIRAL ANTENNA FOR SUBSURFACE RADAR APPLICATIONS

Lim Teck Yong
Senior Member of Technical Staff, DSO National Laboratories
Bachelor of Technology (Hons), National University of Singapore, 1999

Submitted in partial fulfillment of the
requirements for the degree of

MASTER OF SCIENCE IN ENGINEERING SCIENCE
(ELECTRICAL ENGINNERING)

from the

NAVAL POSTGRADUATE SCHOOL
December 2003

Author: Lim Teck Yong

Approved by: David Jenn
Thesis Advisor

Jeffrey B. Knorr
Second Reader

John P. Powers
Chairman, Department of Electrical and Computer Engineering

THIS PAGE INTENTIONALLY LEFT BLANK

ABSTRACT

Subsurface radar, also known as ground-penetrating radar is increasingly being used for the detection and location of buried objects such as mines and structures that are found within the upper regions of the earth's surface. The thesis gives a review of the work done to date in this area, laying emphasis on the possible antenna designs to match the range of intended applications. An overall design strategy is outlined, together with a more detailed treatment of the ground-penetrating radar subsystems and topics which are relevant to effective subsurface radar operation. These include the dielectric properties of earth materials, the choice of the frequency of operation, as well as the design and construction of suitable antennas.

Finally, a new antenna structure called the counter-wound spiral antenna, which is suitable for subsurface radar applications, is examined. The counter-wound spiral antenna has a broad bandwidth and a linear polarization with a controllable plane of polarization from a planar geometry. It has an electronically steerable plane of polarization. This unique property offers a reduction in antenna polarization loss and allows the extraction of maximum information from the target scattered echo.

THIS PAGE INTENTIONALLY LEFT BLANK

TABLE OF CONTENTS

THIS PAGE INTENTIONALLY LEFT BLANK

LIST OF FIGURES

LIST OF TABLES

THIS PAGE INTENTIONALLY LEFT BLANK

ACKNOWLEDGMENTS

This thesis is dedicated to my loving wife, Sharon, for accompanying me in my research here at the Naval Postgraduate School. I deeply appreciate the love, consideration, and unrelenting support given to me throughout my studies here.

I would like to express my sincere appreciation to my advisor, Professor David Jenn and second reader, Professor Jeffrey Knorr. Without their support and supervision, this thesis would not have been possible.

Lastly, I must thank my sponsor, DSO National Laboratories, for providing me with this opportunity to pursue my postgraduate study here at the Naval Postgraduate School.

THIS PAGE INTENTIONALLY LEFT BLANK

EXECUTIVE SUMMARY

Subsurface radar or ground-penetrating radar (GPR) refer to a wide range of electromagnetic techniques designed primarily for the location of objects or interfaces buried beneath the earth's surface. These techniques offer rapid, high resolution and non-invasive investigation of underground objects and structures by recording microwave radiation that passes through the ground, reflects from the buried objects or interfaces and is then returned to the surface.

The operational effectiveness of the subsurface radar depends on the (*i*) efficient coupling of electromagnetic radiation into the ground; (*ii*) adequate penetration of the radiation through the ground having regard to target depth; (*iii*) ability to obtain from buried objects, or other dielectric discontinuities, a sufficiently large scattered signal for detection at or above the ground surface; and (*iv*) an adequate signal bandwidth in the detected signal with regard to the desired resolution and noise levels.

In GPR applications, very often the antenna is placed directly over the ground with its axis normal to the surface without contacting the surface of the earth. This allows rapid surveying of the subsurface during operation. For this application, antennas with uniform properties such as input impedance, gain, and polarization over a wide bandwidth are desirable, especially when the transmitted and received signal has a very large signal bandwidth.

It has been observed experimentally that the attenuation of electromagnetic waves increases with frequency and that for a particular frequency, wet materials exhibit higher attenuation as compared to dry ones. Variations in electrical properties of ground materials cause reflections. It is the reflections from buried objects that propagate back to the surface that are recorded by the subsurface radar.

The requirements of the antenna designed for subsurface radar application can be quite different from those that are used for atmospheric telecommunication purposes. The subsurface radar antenna has to be matched to the characteristics of the propagation medium as well as the geometrical shape of the target.

The impulse response, fractional bandwidth and polarization state of the antenna are some of the critical parameters being considered. The cross-coupling levels between the closely spaced transmitter and receiver, the interaction between the reactive field of the antenna and the propagation medium as well as the geometry (as in planar or non-planar) of the antenna are also important considerations.

The spiral antenna, which belongs to the class of frequency-independent antennas, has radiation pattern, impedance and polarization that remain virtually unchanged over a large bandwidth. An ideal spiral antenna that radiates a circularly polarized wave towards the air/ground interface will not receive the wave reflected from the interface, because it is predominantly cross-polarized. When used for detection of objects such as a rod that scatters a linearly polarized wave, the spiral antenna only receives the co-polarized half of the backscattered power, therefore reducing the probability of target detection.

For counter-wound spiral antenna (CWSA), the polarization of the wave transmitted by the antenna can be made either vertically or horizontally polarized by varying the delays to the signals that are being sent to the antenna feeds of the spirals. This design allows buried objects to be detected by both vertically and horizontally polarized waves, which results in reduced polarization loss. This enables better detection and identification of targets which lie in any arbitrary orientation with respect to the main antenna axis.

Several important aspects of the performance of the CWSA have been verified through simulations. It has been shown that the rotated CWSA (with the plane of the front and rear spiral antenna planes rotated 90 degrees to each other along the main antenna axis), gives a better performance in terms of reflections as compared to the unrotated case. The CWSA far field polarization has also been verified to be linearly polarized when an appropriate delay is set to the excitation input of the front planar antenna. The plane of polarization of the linearly polarized wave can be changed by varying the signal excitation delay. The research work has resulted in the successful design of a CWSA that has a broad bandwidth and linear polarization with an electronically controllable plane of polarization from a planar geometry.

I. INTRODUCTION

The terms subsurface radar or ground-penetrating radar (GPR) refers to a wide range of electromagnetic techniques designed primarily for the location of objects or interfaces buried beneath the earth's surface. These techniques offer rapid, high resolution and non-invasive investigation of underground objects and structures by recording microwave radiation that passes through the ground and is returned to the surface. Virtually all systems developed in recent years to detect landmines and buried unexploded ordinance (UXO) have included ground-penetrating radar (GPR) as one of the principle subsystems. GPR is currently one of the leading sensor technologies the U.S. Army is investigating for the detection of sub-surface landmines. Planning System Inc, has developed working stepped frequency GPR systems that operate over the frequency band of 800 MHz to 4 GHz, using different variations of log spiral and Archimedean spiral antennas [1].

In a typical GPR, a transmitter sends a microwave signal into the subsurface which will be reflected by the buried objects or interfaces beneath the earth's surface. The microwaves propagate at velocities that are dependent upon the dielectric constant of the subsurface medium. Changes in the dielectric constant that are due to changes in the subsurface materials cause the radar wave to be reflected. The time taken for the energy to return to the surface is related to the depth at which the energy was reflected. Thus interpretation of this reflected energy yields information on structural variation of the subsurface.

The design of GPR is largely applications-oriented and the overall design philosophy is usually dependent on the target type and the obscuring medium. For example, the choice of GPR operating frequency is correlated to the expected depth of penetration of the microwave signals and the required ground vertical resolution. Higher frequency sources will offer greater vertical resolution of structure, but will not penetrate as deep as lower frequency sources.

The range of applications of subsurface radar methods is growing, along with the sophistication of signal recovery techniques, hardware designs and operating practices,

with the last including airborne and satellite surveying. GPR is the only geophysical technique that can offer the horizontal and vertical resolution necessary for many ground probing applications. This includes hydrological and geotechnical applications such as determining soil and bedrock characteristics in the shallow interface, as well as high-resolution imaging for monitoring structure integrity of buildings, mine walls, roadways and bridges.

The first description of the use of electromagnetic signals to determine the location of buried objects was found in a German patent by Leimbach and Lőwy [2] in 1910. Their technique consisted of burying dipole antennas in an array of vertical boreholes and comparing the magnitude of signals received when successive pairs were used to transmit and receive. The main feature of this technique is the use of continuous wave (CW) together with diffraction effects of buried objects or underground features. Scattering from objects are due to variation in the conductivity of the subsurface medium.

The first use of pulsed techniques to determine the structure of buried features appears to originate from the work of Hűlsenbeck in 1926 [3]. Pulsed techniques were then extensively developed over the years as a means of probing to considerable depths in subsurface media including ice, fresh water, salt deposits, desert sand, and rock formations. A more extended account of the history of subsurface radar and its growth up to about 1976 is given by Daniels [4] and Nilsson [5].

Alternative techniques that have been used for detecting buried objects or underground structures include the seismic method and the use of sonar in marine environments. Seismic methods are used extensively for the exploration of deep geographical features. Other methods include resistivity and magnetometry surveying, as well as low-frequency induction for detecting localized shallow metal objects or deeper metallic pipes and cables. The preferred method to be used depends on the target type, the nature of the immersing material as well as the operational requirements. For detection of non-metallic targets, a seismic method is a good alternative to subsurface radar.

One of the operational advantages of using subsurface radar techniques is its ability to perform rapid surveying of the subsurface. This is due to the absence of contact be-

tween the antenna and the surface of the earth. The GPR antenna can also be designed to achieve adequate bandwidth to suit its intended application.

In a GPR applications, very often the antenna is placed directly over the ground with its axis normal to the surface without contacting the surface of the earth. This allows rapid surveying of the subsurface during operation. For this application, antennas with uniform properties such as input impedance, gain, and polarization over a wide bandwidth are desirable, especially when the transmitted and received signal has a very large bandwidth. The two-arm equiangular spiral antenna discussed here has these frequency-independent characteristics in free space, and these characteristics are preserved to a great degree when placed over the ground. Olhoeft [6] discussed several applications and frustrations in using ground-penetrating radar system.

This thesis presents a review of subsurface radar, highlighting those features which differ from conventional atmospheric radar techniques and emphasizing the interrelationship between those topics in electromagnetism, soil science, geophysics and signal processing, which form a critical part of the design of a GPR system. A detailed discussion of the design of a two-arm frequency-independent equiangular spiral antenna is presented, showing the important antenna characteristics. A simple design of a 4-arm spiral antenna and its characteristics is then discussed.

The thesis is organized as follows. Chapter II gives a review of the work done to date in the area of subsurface radar, the overall design strategy together with a more detailed treatment of the ground-penetrating radar subsystems and topics which are relevant to effective subsurface radar operation. These include the dielectric properties of earth materials, signal modulation schemes and design and construction of suitable antennas.

Chapter III gives a detailed discussion of the construction of a dual-arm frequency-independent planar spiral antenna, comparing its performance with the theory. Chapter IV presents the design of counter-wound spiral antenna, illustrating its performance with simulation results from Microwave Studio. Chapter V presents a summary and proposes prospective developmental work in this arena.

THIS PAGE INTENTIONALLY LEFT BLANK

II. OVERVIEW OF SUBSURFACE RADAR TECHNIQUES

This chapter examines the principal features affecting the operation and design of a ground-penetrating radar. The descriptions here are mainly qualitative. More detail design information can be found in the technical papers referenced.

The monostatic radar technique is usually employed to detect back-scattered radiation or reflection from a buried target. Although forward scattering of the target can also be used, it is seldom employed due to the need for at least one antenna to be buried and some kind of image transformation to be applied to the measured data. All of the work discussed here is based on target backscattering measurement.

Figure 1 shows the block diagram of a general subsurface radar system. The design is typical of a base-band, sub-surface pulsed radar system. The subsurface radar system records microwave radiation that passes through the ground and is returned to the surface. A transmitter sends a microwave signal into the subsurface. As the radar wave propagates at a velocity that is dependent upon the dielectric constant of the subsurface medium, changes in the dielectric constant that are due to changes in the subsurface materials will cause the radar wave to reflect. The time it takes for the electromagnetic energy to return to the surface is related to the depth at which the energy was reflected. Interpretation of this reflected energy yields information on structural variation of the near subsurface or the depth of the buried objects.

Separate broadband antennas are usually used for transmission and reception. The design options available are usually dictated by the electromagnetic properties of the ground, while the target type and shape will affect the choice of antenna type and configuration as well as the kind of processing techniques to be employed. The effects of the ground on the antenna can be largely decoupled from the rest of the problem and solved independently.

The operational effectiveness of the subsurface radar depends on (*i*) the efficient coupling of electromagnetic radiation into the ground; (*ii*) adequate penetration of the radiation through the ground having regard to target depth; (*iii*) the ability to obtain from

buried objects, or other dielectric discontinuities, a sufficiently large scattered signal for detection at or above the ground surface; and (*iv*) an adequate signal bandwidth in the detected signal with regard to the desired resolution and noise levels. The propagation loss, clutter characteristics and target characteristics described here are distinctly different from those of the conventional free-space radar system [4], and the tradeoffs involved are significantly different.

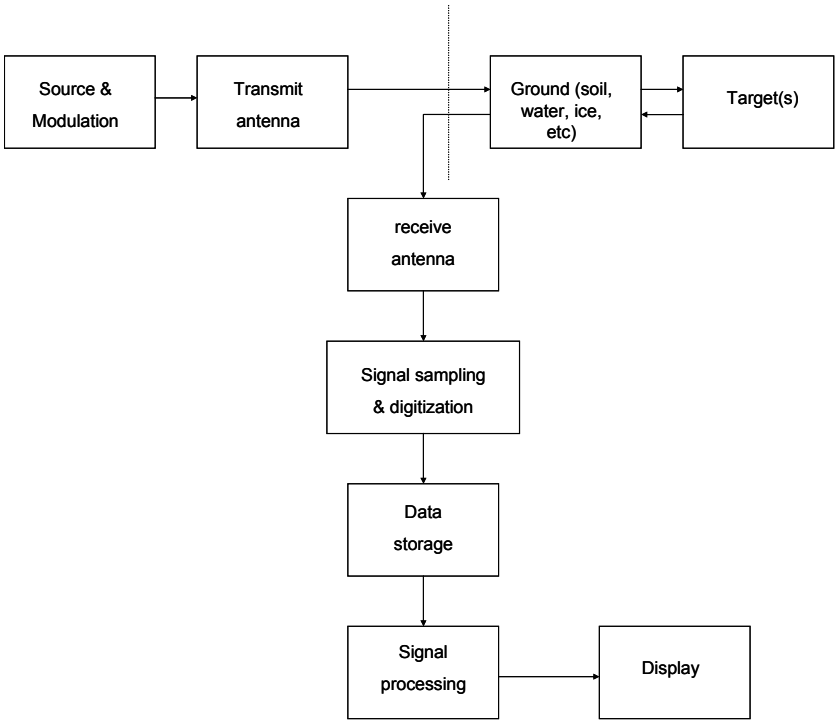

Figure 1. Block diagram showing the operation of a typical base-band subsurface radar system (From Ref. [4].).

The quasi-monostatic geometry of the subsurface radar is shown in Figure 2. The transmitting and receiving antenna are located at almost the same elevation above the ground at which the object/scatterer is buried. The antenna transmits an incident field towards the ground. This field is partially transmitted into the ground and partially reflected from the air/ground interface. The wave that is transmitted into the ground is then scattered by the buried object. In the figure, σ_t represents the radar cross section (RCS) of the target, *R* is the slant range, *d* is the depth of the buried object, *Tx* and *Rx* are the

transmitting and receiving antennas respectively, and θ is the incident angle of the transmitted wave measured from the *z*-axis.

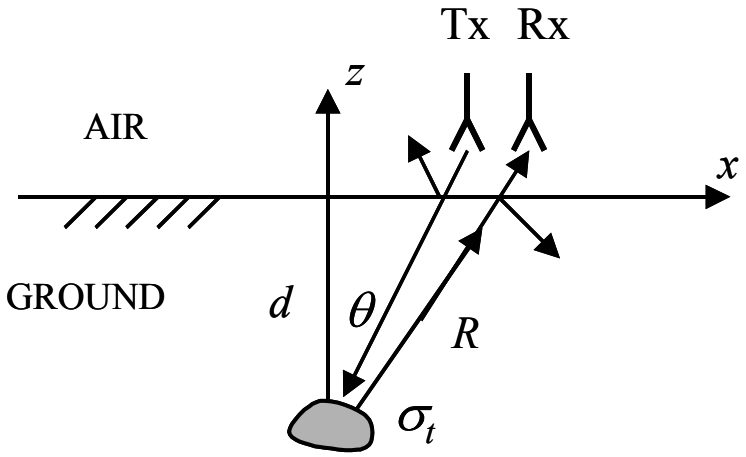

Figure 2. Quasi-monostatic geometry of a typical subsurface radar system (From Ref. [7].).

A. DIELECTRIC PROPERTIES OF EARTH MATERIALS

Ground material can be described by its electrical properties such as electric permittivity (ε), electric conductivity (σ) and magnetic permeability (μ). Since most of the earth's material is non-magnetic, the permeability of the medium can be approximated as the permeability of free space ($\mu = \mu_0$). The conductivity of the medium determines the amount of energy lost from currents induced in the medium by the propagation wave.

The ground materials are generally complex, and losses can arise from both conduction and displacement currents. In the first case, ohmic loss is conventionally expressed in terms of the material conductivity, whereas for a dielectric, a complex permittivity is used. When both losses are present (for example, in wet sand) the losses are not kept separate, but lumped together in either an equivalent conductivity or equivalent permittivity.

Therefore several different representations are possible. Complex permittivity (ε) and complex conductivity (σ) can be defined as follows

complex permittivity $\varepsilon = \varepsilon' - j\varepsilon''$ (1a)

complex conductivity $\sigma = \sigma' - j\sigma''$ (1b)

effective permittivity $\varepsilon_e' = \varepsilon' - \sigma''/\omega$ (2a)

effective conductivity $\sigma_e' = \sigma' + \omega\varepsilon''$ (2b)

imaginary effective permittivity $\varepsilon_e' = \varepsilon'' + \sigma'/\omega$ (2c)

imaginary effective conductivity $\sigma_e'' = \sigma'' + \omega\varepsilon'$. (2d)

When measurements are made on a conducting dielectric, the parameters measured are the apparent permittivity $(\tilde{\varepsilon})$ and the apparent conductivity $(\tilde{\sigma})$, defined as

$$\tilde{\varepsilon} = \varepsilon_e' - j'\varepsilon_e \tag{3a}$$

$$\tilde{\sigma} = \sigma_e' - j\sigma_e''. \tag{3b}$$

The effective electric loss tangent $(\tan\delta_e)$ is given by

$$\tan\delta_e = \frac{\sigma' + \omega\varepsilon''}{\omega\varepsilon' - \sigma''} = -\frac{\sigma_e'}{\sigma_e''} = \frac{\varepsilon_e''}{\varepsilon_e'} = \frac{\sigma_e'}{\omega\varepsilon_e'}. \tag{4}$$

The measurements of interest for making an assessment of a material type for subsurface radar applications are its attenuation (α) and the velocity of wave propagation (υ) as a function of frequency. The relationship between these parameters and the apparent permittivity $(\tilde{\varepsilon})$ is given by the equation

$$\gamma = \alpha + j\beta = j\omega\sqrt{\tilde{\varepsilon}\mu}. \tag{5}$$

The dielectric constant defines the index of refraction of the medium and is the material constant which controls the phase velocity of the electromagnetic waves in the

material. When the permeability is taken to be the permeability of free space (μ_o), the wave velocity is given by

$$\upsilon = c\left[\frac{\varepsilon'_e}{2\varepsilon_o}(\sqrt{1+\tan^2\delta_e}+1)\right]^{-1/2} \tag{6}$$

where c is the speed of light in air. From (2), changes in the subsurface material will affect the index of refraction, and reflected energy will be produced related to the contrast in the dielectric constant across the boundary between the two materials.

The attenuation constant is given by

$$\alpha = \frac{\omega}{c}\left[\frac{\varepsilon'_e}{2\varepsilon_o}\left(\sqrt{1+\tan^2\delta_e}-1\right)\right]^{\frac{1}{2}} \tag{7}$$

or

$$\alpha\left[\text{dB/m}\right] = 129 f\sqrt{\varepsilon'_{er}}\left[\sqrt{(1+\tan^2\delta_e)}-1\right]^{1/2} \tag{8}$$

where f is in GHz $\left(\omega = 2\pi f\right)$.

Table 1 shows the dielectric constant of some common earth materials. The dielectric constant of the medium depends principally on the water content. The reason is that at lower frequencies, water has a relative permittivity of about 80, while for the solid constituents of most soils, ε_r is in the range of 2 to 6. The measured ε_r of soil was found to be in the region of 4 to 40 [1].

Material	Dielectric Constant	Propagation Velocity (m/ns)
Air	1	0.3
Water	81	0.033
Granite	9	0.10
Limestone	6	0.12
Sandstone	4	0.15
Rocks	4~12	0.15~0.087
Dry sand	4~6	0.15~0.12
Wet sand	30	0.055
Dry clay	8	0.11
Wet clay	33	0.052
Dry soils	3~8	0.17~0.11
Wet soils	4~40	0.15~0.047
Asphalt	3~6	0.17~0.12
Concrete	9~12	0.10~0.087

Table 1. Typical dielectric constant of common soil medium and velocity of wave propagation (From Ref. [1].).

It has been observed experimentally that, for most materials that make up the earth near its surface, the attenuation of the electromagnetic radiation increases with frequency. In general, wet materials exhibit higher loss than dry ones at a given frequency. Figure 3 below shows the one-way path loss for different material surfaces over a frequency range from 1 MHz to 1 GHz. It is shown here that the attenuation of wet rock is higher than dry rock, and salt water has the highest level of attenuation.

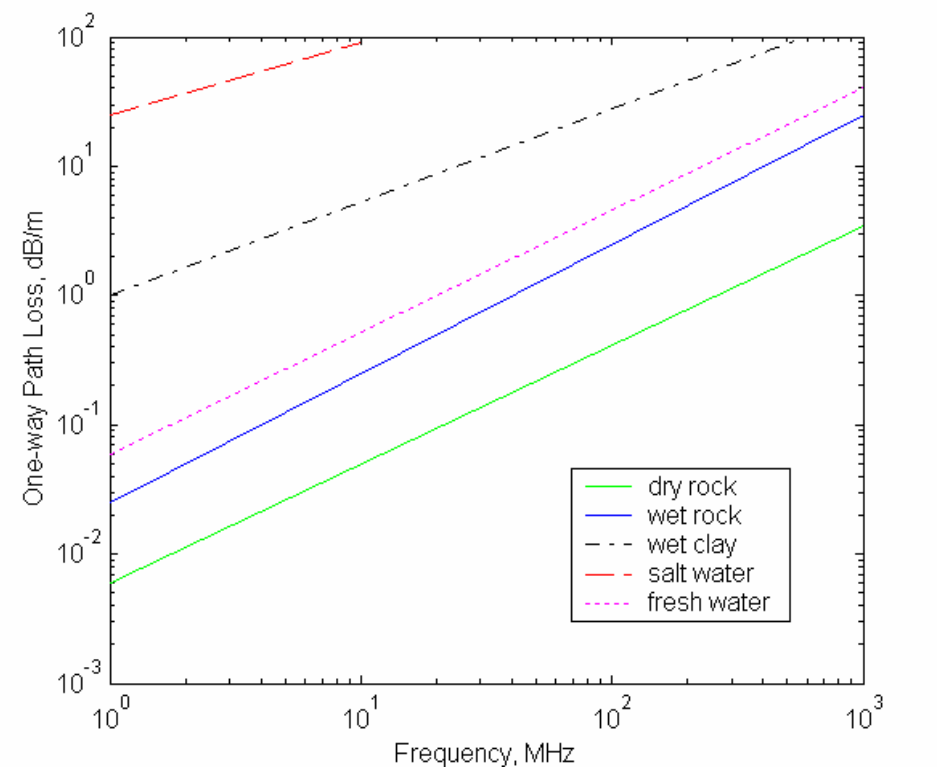

Figure 3. One-way path loss for different surface materials over 1 GHz frequency range (After Ref. [7].).

There is sufficient information to enable a realistic assessment to be made of the likely range of dielectric properties to be encountered when a subsurface radar is being designed for work in a particular environment. Table 2 gives an account of published work relating either to the experimental or the theoretical studies of the dielectric nature of a range of material.

Variations in electrical properties cause reflections at high frequency. The theory of how the reflected waves and the transmitted (refracted) waves propagate away from the boundary of different media is given by Snell's Law. It is the reflections from buried objects that propagate back to the surface that are recorded by the subsurface radar.

Material	Research Area /References
Water, ice, snow	Properties of water in solid and liquid state, King & Smith [8].
	Frequency dependence of water dielectric properties, Potter [9].
	The complex-dielectric constant of sea-ice at frequencies, Vant [10].
	Snow properties effects on millimeter-wave backscatter, Larry [11].
	Loss-Factor behavior of freshwater ice, Georgi [12].
Rock, minerals	Dielectric properties of rocks, King & Smith [8].
	Data on dielectric properties of rocks, Parkhomenko [13], Keller [14], Ulaby [15].
	Radio Propagation at 900 MHz in underground coal mines, Zhang [16].
	Dielectric properties of salt deposits, Unterberger [17]
Soils	Low frequency (<100 Hz) soil dielectric characterization, Dmitriev[18], Fano [19].
	Moisture Effects on the dielectric properties of soils, John [20].
	Dielectric Properties of soils in the 0.3-1.3 GHz , Neil [21].
	Complex dielectric constant of wet and frozen soil, Tikkhonov [22].

Table 2. Published work relating to the experimental and theoretical studies of the dielectric properties of a range of materials.

B. DEPTH AND FREQUENCY OF OPERATION

Subsurface radar systems usually operate in the megahertz range. The waves that propagate into the ground will have wavelengths on the order of 1 meter or less. The horizontal and vertical resolutions of the radar images are dependent upon the wavelength of operation, such that the smaller the wavelength, the better the resolution. The higher frequency source will, therefore, yield better resolution, but the higher frequency signals will not penetrate as deep as the lower frequencies. For a given signal detection threshold the maximum depth of investigation decreases rapidly with increasing frequency. Thus a careful choice of frequency of operation must be made based on the expected target depth and the system design goals.

Table 3 shows the typical required penetration depths of a range of materials, and their appropriate upper operating frequencies. A consideration which applies when choosing an operating frequency for detecting localized objects, rather than interfaces between thick layers, is the fact that the backscattered amplitude is also frequency dependent and, apart from any resonance effects, decreases with decreasing frequency.

It can be concluded from Table 3 that subsurface radar operating in the 100 MHz to 1 GHz frequency range has a penetration depth of about 2 to 3 meters into the different types of soils (clay, loam and sand). This will be the typical operating frequency range of most subsurface radars that are used for mine detection.

In longer range (deeper) investigation of geological structure or deep ice, frequencies as low as a few tens of MHz are used. This is as shown in the case of 20 meters of rock or coal, with the radar operating at a much lower frequency in the 50 MHz to 500 MHz range.

The deepest penetration therefore occurs in dry, non-clay soils, and in dry rocks with no clay cementation. Snow and ice cover will have little effects on GPR data collection. When the soils or rocks are saturated, the conductive nature of the filling liquid becomes important. A consideration when choosing an operating frequency for the detection of localized objects rather than interfaces is that the backscatter from the targeted

object is also frequency dependent. The amplitude of the backscatter will also decrease with increased frequency of operation.

Material	Penetration depth	Max. Operating Freq
Cold pure fresh water ice	10 km	10 MHz
Temperate pure ice	1 km	2 MHz
Saline ice	10 m	100 MHz
Fresh Water	100 m	100 MHz
Sand (desert)	5 m	1 GHz
Sandy soil	3 m	1 GHz
Loam soil	3 m	500 MHz
Clay soil	2 m	100 MHz
Salt (dry)	1 km	250 MHz
Coal	20 m	500 MHz
Rocks	20 m	50 MHz
Walls	0.3 m	10 GHz

Table 3. Depths at which radar probing gives useful information, taking into account the attenuation encountered and the nature of the reflectors (From Ref [4].).

C. DEPTH RESOLUTION

The depth resolution required for the subsurface radar is dependent on its intended application. In situations where only the depth of the interface is of interest, the radar may only need to operate at a single frequency. The depth of the interface can be determined by measuring the time delay of the returned echoes. This technique is often known as radio echo sounding.

For detection of specific buried objects such as mines or buried pipes, a larger bandwidth is required in order to be able to distinguish between the various scatterers. The earth, which acts as a low pass filter, would modify the spectrum of the transmitted signal according to its material properties. This effect of a frequency-dependent attenuation of the electromagnetic waves by the ground limits the information bandwidth of the received signal at a given noise or clutter level.

Figure 4 shows the spectral spread of a stepped frequency waveform (12 pulses, frequency step size 50 MHz per pulse, start frequency 500 MHz, PRF 10 MHz, pulse width 0.01 microsecond) being transmitted and received from a target buried underground.

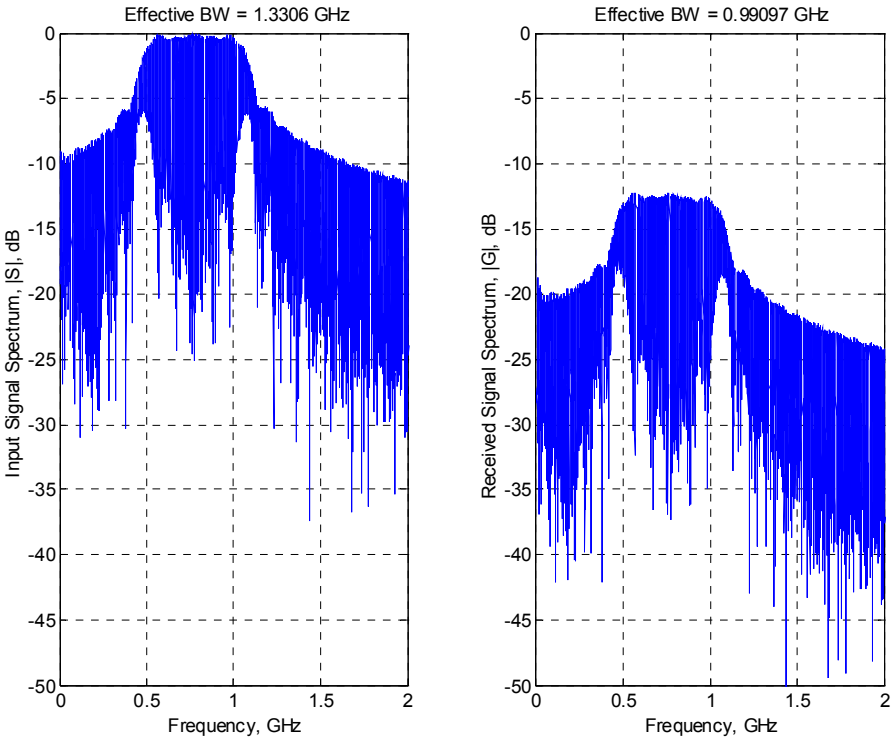

Figure 4. Frequency spectral spread of a stepped frequency waveform being transmitted into and received from the ground (After Ref. [7].).

From Figure 4, it can be observed that the ground loss has reduced the effective bandwidth B_e by about 25%, where B_e is given by

$$B_e^{\,2} = \frac{1}{E}\int_{-\infty}^{\infty}(2\pi f)^2\left|S(f)\right|^2 df\,, \tag{9a}$$

where E is the signal energy and the range resolution of the radar is approximated by

$$\Delta R \approx \frac{c}{2}\tau_e\,, \tag{9b}$$

where τ_e is the effective pulse width. The ground loss has also caused an increase in the range cell by about 25%.

D. HORIZONTAL RESOLUTION

The horizontal resolution of the subsurface radar is important when localized targets of the same depth are being sought and distinguished. The technique employed to obtain horizontal resolution depends on the wave attenuation of the medium. The locations of the transmitter and receiver, as to whether they are collocated or physically separated, will have to be known.

The horizontal resolution of the subsurface radar can be found in several ways. One is based on the power distribution of the received signals from the scatterers as the radar moves over the buried target. Figure 5 shows a collocated transmitter and receiver pair being scanned along the ground surface above a buried object at depth d, with the one way voltage attenuation constant of the medium as α. The monostatic case is shown with the incidence angle of the transmitted wave measured from the z-axis denoted as θ.

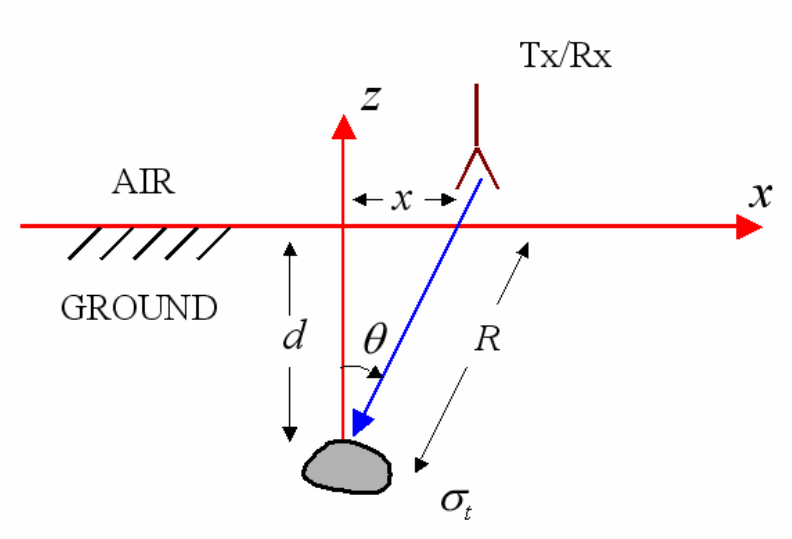

Figure 5. Geometry for estimation of the horizontal resolution of subsurface radar (From Ref. [7].).

The slant range R can be calculated if the depth d of the buried object and the distance x from the z-axis, directly above the buried object is known. Range R is given by

$$R = \sqrt{d^2 + x^2} \ . \tag{9}$$

The field (voltage) attenuation constant of the medium α is

$$\alpha = -\ln(10^{-L/20}) \, , \tag{10}$$

where L is the " loss in dB per meter" of the medium, and is related to the attenuation constant by the equation

$$L = 20\log\left(\frac{E \text{ at 1 m depth}}{E \text{ at surface}}\right) = 20\log\left(e^{-\alpha \cdot 1}\right). \tag{11}$$

Assuming an inverse fourth power of decay of received signal power with target depth (i.e., the monostatic case), the signal received from the target varies as

$$P_r \propto \frac{e^{-4\alpha R}}{R^4} \, . \tag{12}$$

Figure 6 shows the return from a target at depth d = 2 m, with the radar moving on the ground along the x-axis. It shows the normalized power received from the target for three ground attenuation values. Figure 7 shows the returns from two equal RCS targets positioned at x = 0 and x = 2 m, both at depth d = 2 meters. The normalized received powers from different position of x for two different ground losses of 3 dB/m and 10 dB/m were simulated. It was observed that higher ground loss would actually improve the horizontal resolution. Therefore, increasing the loss per meter of the medium has the same effect as narrowing the antenna beamwidth, resulting in better horizontal resolution.

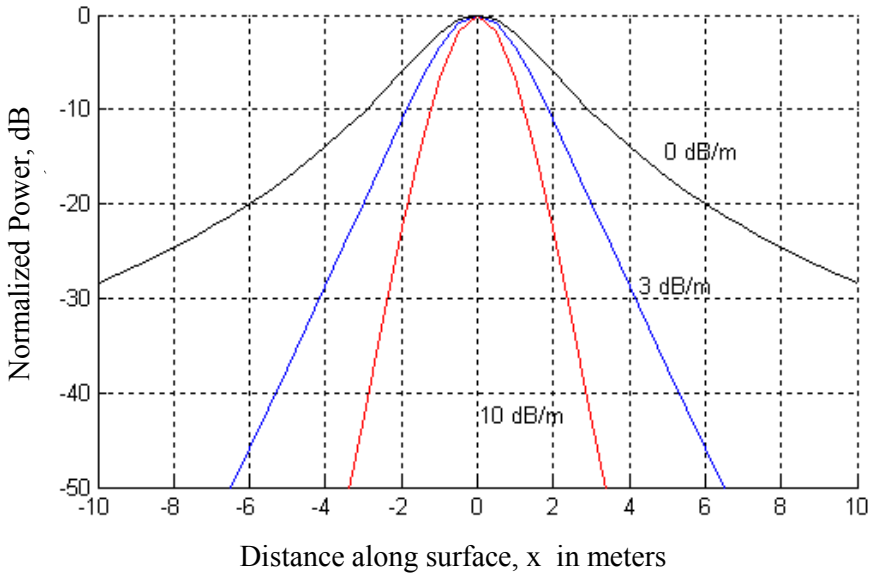

Figure 6. Power received from target at depth (d = 2 m) for varying values of distance x away from the target in three types of ground losses (After Ref. [7].).

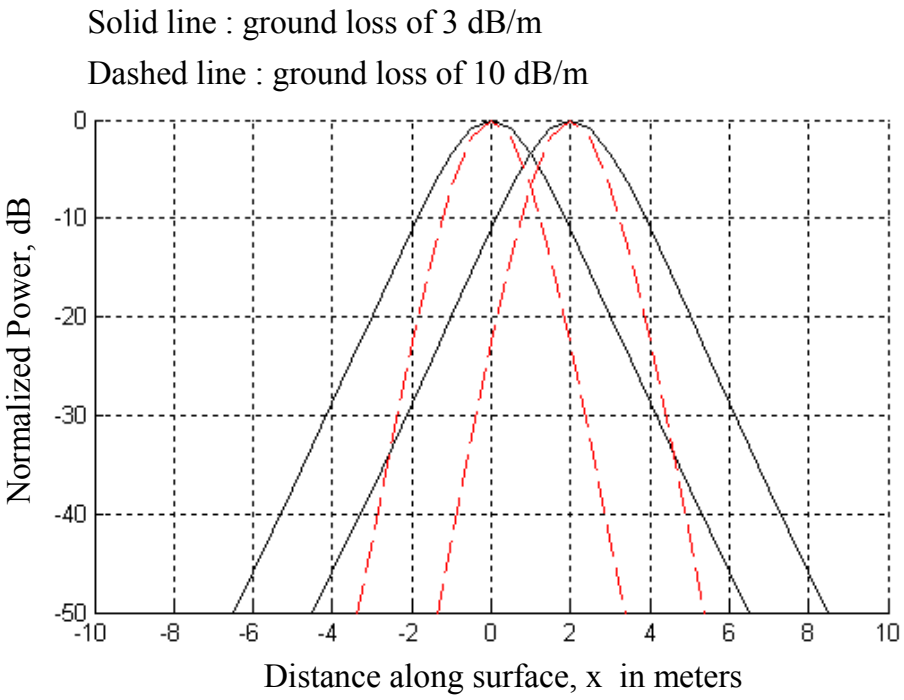

Figure 7. Power received from 2 target at depth (d = 2 m) and separated by x = 2 m, for ground loss of 3 dB/m and 10 dB/m (After Ref. [7].).

E. FREQUENCY-INDEPENDENT ANTENNAS

The requirements of an antenna designed for subsurface radar application can be quite different from those that are used for atmospheric telecommunication purposes. The subsurface radar antenna has to be matched to the characteristics of the propagation medium as well as the geometrical shape of the target.

The impulse response, fractional bandwidth, and polarization state of the antennas are some of the critical parameters being considered. The cross-coupling levels between the closely spaced transmitter and receiver, the interaction between the reactive field of the antenna with the propagation medium as well as the geometry (as in planar or non-planar) of the antenna are also important considerations.

As attenuation of radio waves in geophysical media (such as soil or ice) increases with frequency [4, 23], better ground penetration is usually achieved by operating the radar at lower frequency. This would however results in bigger size antenna since antenna size are generally proportional to the frequency of operation.

The range resolution of the radar depends on its operating bandwidth. The wider the frequency range of operation, the better would be its range resolution. Thus, to achieve finer range resolution, a broadband antenna is required. Typical ground-penetrating radar with a 500-MHz frequency range of operation would correspond to a radar range resolution of about 15 cm in soil [23]. The lowest frequency of operation is usually a compromise between the media attenuation and the antenna size [24].

Element antennas like monopoles, cylindrical dipoles, bi-conical dipoles and resistively loaded bowtie antennas are characterized by limited bandwidths, low directivity and linear polarization. The antennas are, however, usually small in size, and can be arranged cross-polarized to provide good isolation and effective target discrimination against planar targets. The current distribution of the element antennas can be conveniently approximated by current elements, making the analysis of the radiation characteristics convenient.

A circularly polarized antenna is usually preferred to a linearly polarized antenna because the strength of the reflected wave from the object does not depend on the orienta-

tion of the object relative to the antenna. For a linearly polarized antenna, if the transmitting antenna is cross-polarized to the receiving antenna in order to reduce mutual coupling, the receiving antenna will probably not be able to detect the reflected wave from thin object.

Frequency-independent antennas like the Achimedian (or sometimes known as Archimedes Spiral), equi-angular spiral and conical spiral are all circularly polarized broadband antennas. Dyson [25] discussed the basic differences between the equiangular and Archimedes spiral antenna and their characteristics, such as radiation efficiency and ultimate bandwidth capabilities.

Among the circularly polarized antennas mentioned above, only the conical spiral antenna radiates unidirectionally. However, on the conical spiral antenna, different frequency waves are radiated from different regions of the cone. This gives rise to problems in range measurement, because the distance to the target changes with frequency. Hertel [26] investigated the two-arm conical spiral antenna when it is placed directly over the ground with its axis normal to the surface of the ground. The conical spiral antenna has been shown to have uniform impedance, gain, and circular polarization over a broad frequency range.

Planar antennas like the equi-angular spiral, Achimedian, and log-periodic spiral antennas, shown in Figures 8 through 10 do not have the range measurement problem mentioned earlier. However, the planar antenna is bi-directional. Takashi [24] demonstrated the use of planar spiral antenna with a cylindrical waveguide back to achieve a wideband (500 MHz bandwidth), circular polarization and unidirectional properties. The minimal physical volume of planar antennas is certainly a distinct advantage.

Figure 8. Four-arm logarithmic spiral antenna with self-complementary pattern (From Ref. [4].).

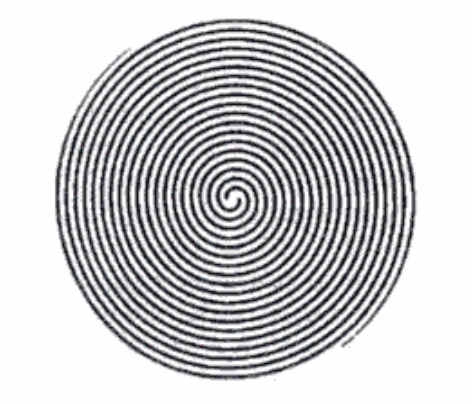

Figure 9. Two-arm Archimedean spiral antenna (From Ref. [4].).

Figure 10. Four-arm planar log-periodic antenna (From Ref. [4].).

Subsurface radar usually employs separate antennas for transmission and reception. This is due to the absence of fast switches to protect the receiver during transmission. The cross-coupling level between the transmitting and receiving antennas (isolation) is an important consideration.

Some of the general design principles of frequency-independent antennas discussed by Rumsey [27] are as follows:

a) The antenna is excited from the end at which the high frequencies electromagnetic waves are radiated.

b) The inactive part of the antenna should produce negligible radiation.

c) The geometry of the antenna should be defined entirely by angles.

Many of the antennas are fed by a balun, to match the unbalanced transmission line to a balanced radiating structure.

Other types of antennas that have been successfully used for subsurface radar applications are traveling-wave antennas and aperture antennas. The classes of antenna that can be used successfully for subsurface radar applications generally require a wide bandwidth and low operating frequency. The choice between a planar and non-planar geometry is more critical when the antenna is required to operate close to the ground surface. The equiangular spiral antenna is useful in cases where an extended impulse response can be accepted but, under conditions when the impulse response must be more limited, the continuously-loaded dipole or traveling-wave antenna is preferred.

F. DATA COLLECTION

The most common type of survey technique used in subsurface radar application is common offset profiling. Other techniques include the common midpoint survey. In the common offset profiling technique, the transmitting and receiving antennas are at a fixed distance and the radar is progressively moved along the line of survey to record backscattered returned signals from the subsurface. With bistatic antennas, the antenna separation (source-receiver offset) has to be held constant for common offset profiling, and this offset can be optimized for best results. For this type of system, the horizontal sample inter-

val is usually chosen to be large which results in reduced lateral resolution. With a monostatic or quasi-monostatic system, both the transmitting and receiving antennas are housed within the same unit. This allows for better horizontal resolution profiling of the subsurface.

In common midway profiling, the two bistatic antennas are progressively moved away from each other, keeping the center between the two antennas fixed a one location. As the antennas are moved away from the origin, the subsurface data is collected at each new, more distant position. Since the electromagnetic wave travel time is directly proportional to the increasing offset between the two antennas, this type of data profiling can help to determine the velocity of the wave in the subsurface.

During data acquisition, multiple data scans are usually taken at each survey location. The data recorded are then added up coherently to remove incoherent noise present in the data samples. The monostatic mode discussed is usually used for rapid surveying in a continuous data profiling mode, whereas the bistatic mode is used for enhanced resolution profiling over discrete locations.

G. DATA PROCESSING

Some basic data processing functions are usually performed on the raw data collected. The time offset due to instrument recording is first removed prior to any data interpretation of the radar images. The ringing due to the close proximity of the source and receiving antennas in monostatic system are then removed. The effects due to non-constant motion along the profile and amplitude variation would have to be compensated. The return signal due to reflections from near objects will naturally have a much higher amplitude as compared to the those objects buried at a much deeper depth. This loss of signal amplitude is due to both the intrinsic attenuation of the soil and the geometric spreading of the signals. Various time-variable gain functions may be applied to compensate for such gain variations in the received signals. Lateral averaging of data by summing data traces received from the subsurface can be used to improve the signal-to-noise ratio of the received signals. Frequency filtering is also used to remove unwanted spurious signals present in the data samples to produce a more interpretable GPR image.

H. SUMMARY

This chapter examined the principal features affecting the operation and design of the ground-penetrating radar and the monostatic radar technique that is usually employed to detect back-scattered radiation or reflection from a buried target.

The operational effectiveness of the subsurface radar depends on several factors such as the efficient coupling and penetration of electromagnetic radiation into the ground and the ability to obtain a sufficiently large and wideband scattered signal.

It has been observed that the attenuation of the electromagnetic radiation increases with frequency for most materials that make up the earth near its surface, and in general, wet materials exhibit higher loss than dry ones at a given frequency.

The classes of antenna that can be used successfully for subsurface radar applications generally require a wide bandwidth and low operating frequency. The spiral antenna is a prime candidate, and its performance will be examined in the next chapter.

THIS PAGE INTENTIONALLY LEFT BLANK

III. SPIRAL ANTENNA DESIGN

The design, characteristics, and performance of the planar spiral antenna is examined in this chapter. The planar spiral antenna has a broad bandwidth and generates circularly polarized waves. These are useful properties for subsurface applications.

A. PLANAR EQUIANGULAR SPIRAL ANTENNA IN FREE SPACE

Frequency-independent antennas refer to antennas that have no theoretical limitation on the bandwidth of operation. In practice, these are antennas whose radiation pattern, impedance and polarization remain virtually unchanged over a large bandwidth [28]. Between the band limits, the performance varies in a manner that is periodic with the logarithm of frequency. These antennas are often also called as logarithmically periodic or log-periodic antennas.

The design of a frequency-independent antenna is based upon the fundamental principle that, if the shape of the antenna were such that it could be specified entirely by angles, its performance would be independent of frequency [29].

This implies that an infinite electrical dimension of such antenna, in order to operate over an infinite frequency range. This means that the current distribution must decrease with distance from the input much more rapidly so that the infinite antenna can be truncated with practically no effect on the radiation pattern [30]. To achieve frequency independence with a practical size antenna (one of finite size), the antenna must consist of active regions. An active region is that part of the antenna that contributes the most to the radiation at one particular frequency. Since this region moves along the antenna as the frequency is changed, its dimensions scale with wavelength and the antenna is able to fulfill the self-scaling and self-complementary conditions over a broad bandwidth.

For the required frequency range of operation, the spiral antenna can be truncated while still retaining the properties of the infinite structures over a very wide bandwidth of operation. The arm length of the antenna need only be of the order of one wavelength at

the lowest frequency of operation for frequency independence. The upper frequency of operation is constraint by the size of the feed region [29].

Dielectric loading could be also be used to reduce the resonant frequency and the physical size of the antenna. This is done by placing a piece of dielectric substrate below the antenna [31]. In general, one is able to achieve better antenna efficiency and larger bandwidth by using a thick substrate with a low dielectric constant, at the expense of larger element size. Similar performance can also be obtained using a thin structure that has a higher dielectric constant.

Rumsey [27] has reviewed a wide range of frequency-independent antennas. The planar and conical equiangular spiral antennas have useful properties for subsurface applications. Both produce circularly polarized radiation while four-element equiangular spirals can be designed to have two orthogonal pairs of elements, so that the use of one pair to transmit and one pair to receive allows the depolarization characteristics of targets such as pipes and tunnels to be exploited.

The planar equiangular spiral antenna is an example of self-complementary structure which enables its impedance to be calculated through Babinet's principle [32]. For any self-complementary structure the antenna input impedance is frequency-independent in the designed bandwidth of operation.

The planar equiangular spiral radiates in both directions perpendicular to the plane of the planar antenna. Absorbing material can be placed at the rear of the planar antenna if a unidirectional radiation pattern is required. Generally, it is not possible to obtain a wide bandwidth using a conducting back plane, because destructive interference between the spiral and its image will occur at some frequencies in the band.

Thaysen [33] discusses the design of a cavity-backed coplanar-strip-fed logarithmic single-plane spiral antenna that covers a 9:1 bandwidth with a return loss better than 10 dB operating from 0.4 GHz to 3.8 GHz.

The electromagnetic simulation program Microwave Studio (developed by CST) was used to analyze the performance of the spiral antenna in terms of its input reflection

coefficients, antenna radiation pattern, and input impedance. The simulated results of the antenna were compared to theoretical results.

B. PLANAR EQUIANGULAR SPIRAL ANTENNA GEOMETRY DESIGN

The design of the equiangular spiral antenna is based upon a simple fundamental principle that if all dimensions of the antenna active regions are changed in linear proportion to a change in wavelength, the performance of the antenna is unchanged except for a change in scale in all measurements of length. The surface of the logarithmic planar spiral antenna can be completely described by angles using the following equations

$$\rho_1 = \rho_0 e^{a\phi} \tag{13a}$$

$$\rho_2 = \rho_0 e^{a(\phi-\phi_0)} \tag{13b}$$

where ρ_1 and ρ_2 are the outer and inner boundaries of the spiral, respectively. The quantity ρ_0 is the initial inner radius of the spiral, a is the growth rate, ϕ is the angular position varying from $0°$ to $540°$ (for 1-1/2 turn spiral arm design), and ϕ_0 is the initial angular displacement between the two spiral arms. These dimensions are as shown in Figure 11.

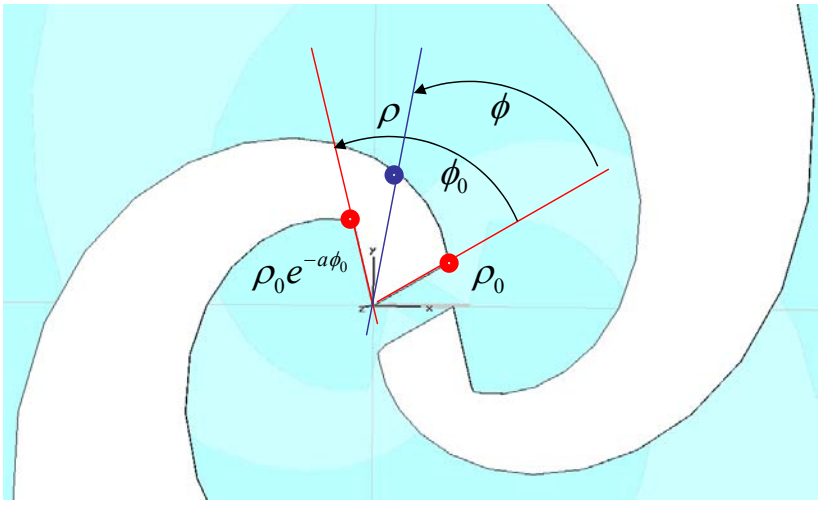

Figure 11. Geometry of the planar equiangular spiral antenna.

Since the spiral antenna was designed using the equation

$$\rho = \rho_0 e^{a\phi}, \tag{14}$$

if the wavelength, λ, is chosen as the unit of the antenna length and if ρ' equals the radial coordinate measured in wavelengths, then

$$\rho' = \frac{\rho}{\lambda} = \frac{e^{a\phi}}{\lambda} = e^{a(\phi - \ln\lambda / a)} = e^{a(\phi - \phi_0)} \tag{15}$$

where

$$\phi_0 = \frac{1}{a}\ln(\lambda). \tag{16}$$

The above result shows that the effect of changing wavelength is equivalent to changing the angle ϕ_0. The active region of the antenna in Figure 12 moves along the spiral towards the ends with decreasing frequency. Consequently, the highest frequency (f_{max}) signal is radiated from the small end of the antenna and the lowest frequency (f_{min}) from the large end. In the simplest approximation, the active region at a given frequency occurs when the spiral is roughly one wavelength in circumference.

The bandwidth (BW) of broadband antennas is often defined as the ratio of the frequencies that mark the bounds of acceptable performance, so the bandwidth of the equiangular spiral is given by

$$BW = \frac{f_{\max}}{f_{\min}}. \tag{17}$$

Experimental and simulation results, however, show that the actual bandwidth is generally lower than that obtained from Equation (17). The radiation pattern of the infinite structure of the spiral antenna is thus independent of frequency except for a rotation in the radiation pattern. This has also been found to be true for the finite length structure [29].

Thaysen [29] has determined a set of design parameters which will give the most frequency-independent radiation pattern and a fairly constant antenna input impedance. The parameters used for the geometry of a single planar spiral antenna were [29]

$$\rho_0 = 2.1\,\text{mm} \tag{18a}$$

$$a = 0.5\,\text{rad}^{-1} \tag{18b}$$

$$\theta_0 = 1.3\ \text{rad}\ (75°). \tag{18c}$$

Figure 12 below shows the planar antenna created in Microwave Studio using the above parameters. The feeds of the two spiral arms were designed to be 2 mm apart.

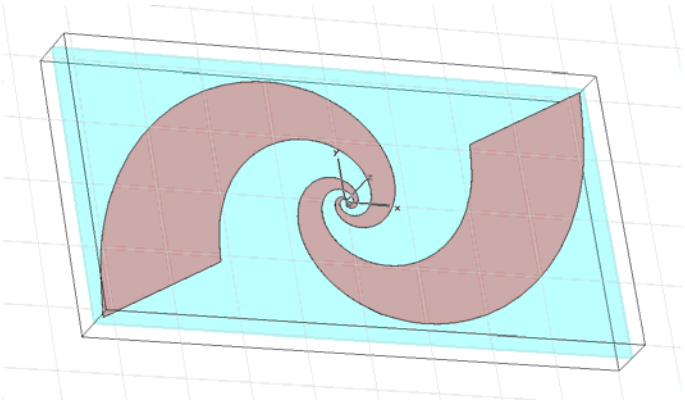

Figure 12. Illustration of a two-arm planar equiangular spiral antenna.

With these design parameters, the widths of the arms have the same dimension as the spacing between the arms. This structure is self-complementary as defined by Babinet's principle [32]. Two structures are self-complementary if one is obtained from the other by exchanging the open and the active regions of the plane.

The input impedance of any plane sheet antenna whose shape is the same as the shape of its complement (except for a trivial change of coordinates) is independent of frequency and is given by

$$Z_{in} = \left(\frac{1}{2}\zeta\right) \tag{19}$$

where $\zeta/2$ is equal to 60π in free space $\approx 188.5\Omega$ [27].

The constant impedance of a self-complementary antenna follows from the relationship

$$Z_1 Z_2 = (60\pi)^2 \tag{20}$$

where Z_1 is the impedance of the antenna, and Z_2 is the impedance of its complementary structure.

The input impedance of the spiral model $(Z_{in} = R + jX)$ is almost resistive, with $(Z_{in} \approx R)$ with R varying between approximately $120\,\Omega$ and $160\,\Omega$. Figures 13 and Figure 14 show the predicted variation of the input impedance of the spiral antenna over the frequency range from 1 GHz to 6 GHz. The difference between theory and simulation is attributed to the finite arm length and the finite antenna plate thickness. Notice that the reactance is small compared to the resistance, allowing the antenna to be well matched to the feeding transmission line over the designed operating bandwidth.

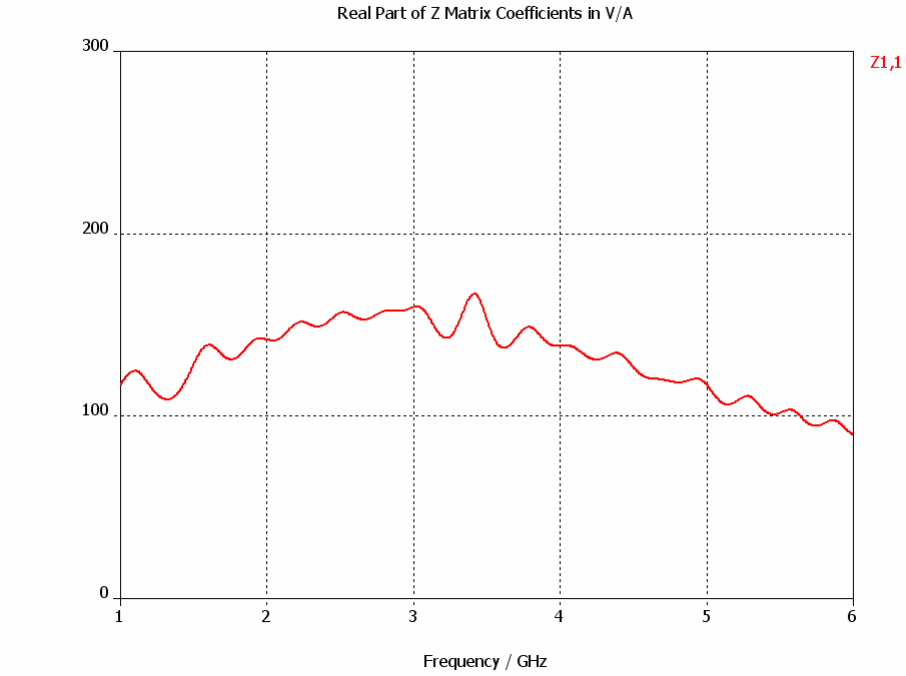

Figure 13. Plot showing the variation of input resistance with frequency predicted using Microwave Studio.

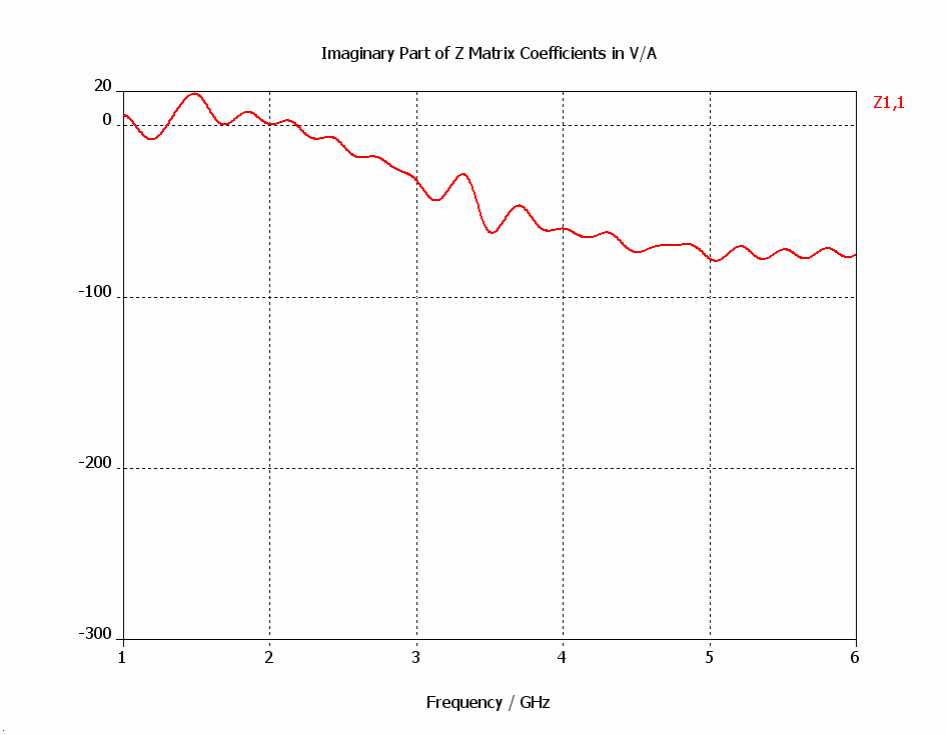

Figure 14. Plot showing the variation of input reactance with frequency predicted using Microwave Studio.

Dyson [29] also discovered that consistently good radiation patterns can be obtained with spirals of only 1-1/4 or 1-1/2 turns, and the antenna pattern has a broad lobe perpendicular to the plane of the antenna. A spiral antenna was designed with two equal dimension arms, each with 1.5 turns. The ends of the two spiral arms were truncated to produce the smallest physical antenna for a given lower resonant frequency. Alternatively, the end of the spiral arms can be tapered, which will result in a more constant input impedance for the antenna [33]. Figure 15 shows the three-dimensional (3-D) radiation pattern of the single planar antenna created. Figures 16 and 17 show the directivity of the antenna for $\phi = 0^o$ and $\phi = 90^o$, respectively.

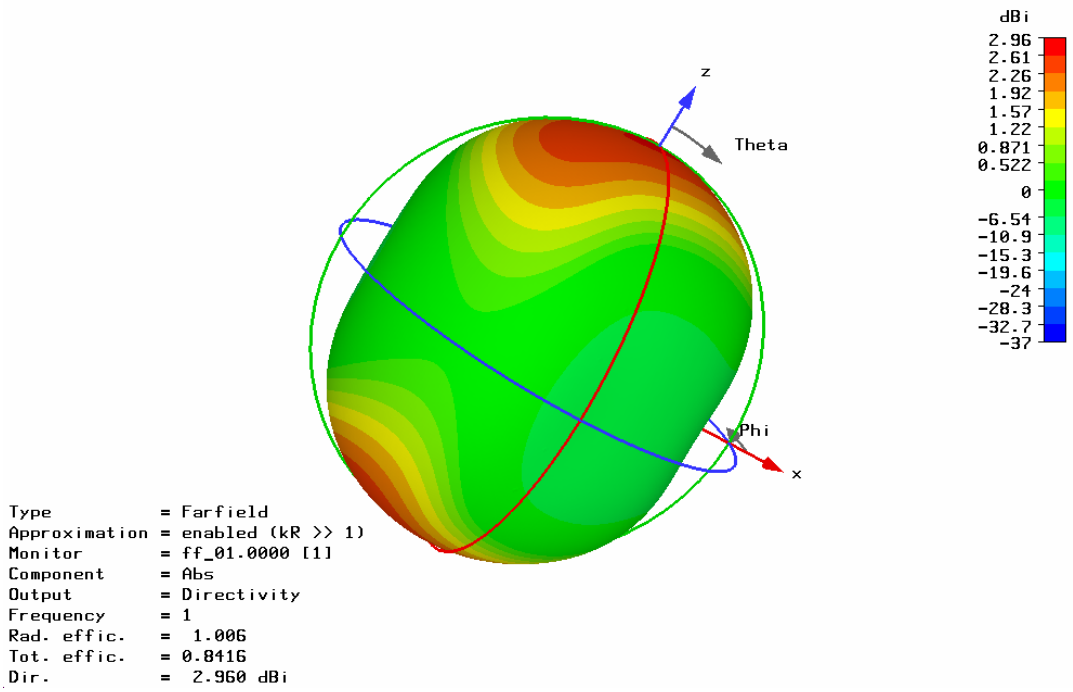

Figure 15. Plot showing the 3-D radiation pattern of the spiral antenna at 1 GHz predicted by Microwave Studio.

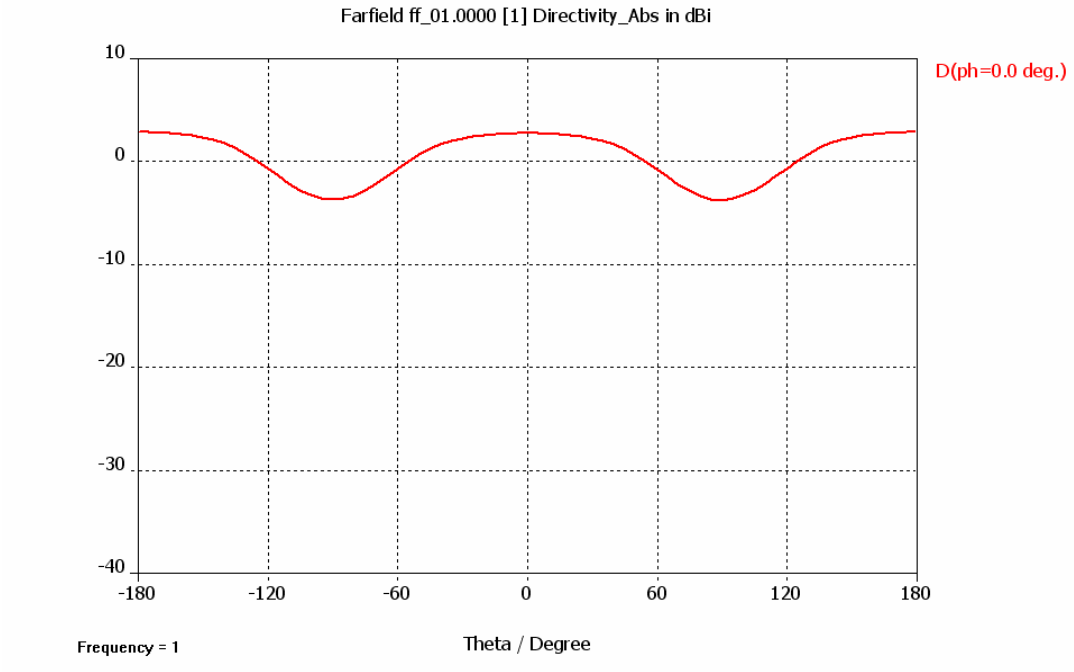

Figure 16. Plot showing the directivity of the antenna for $\phi = 0^o$ as predicted by Microwave Studio.

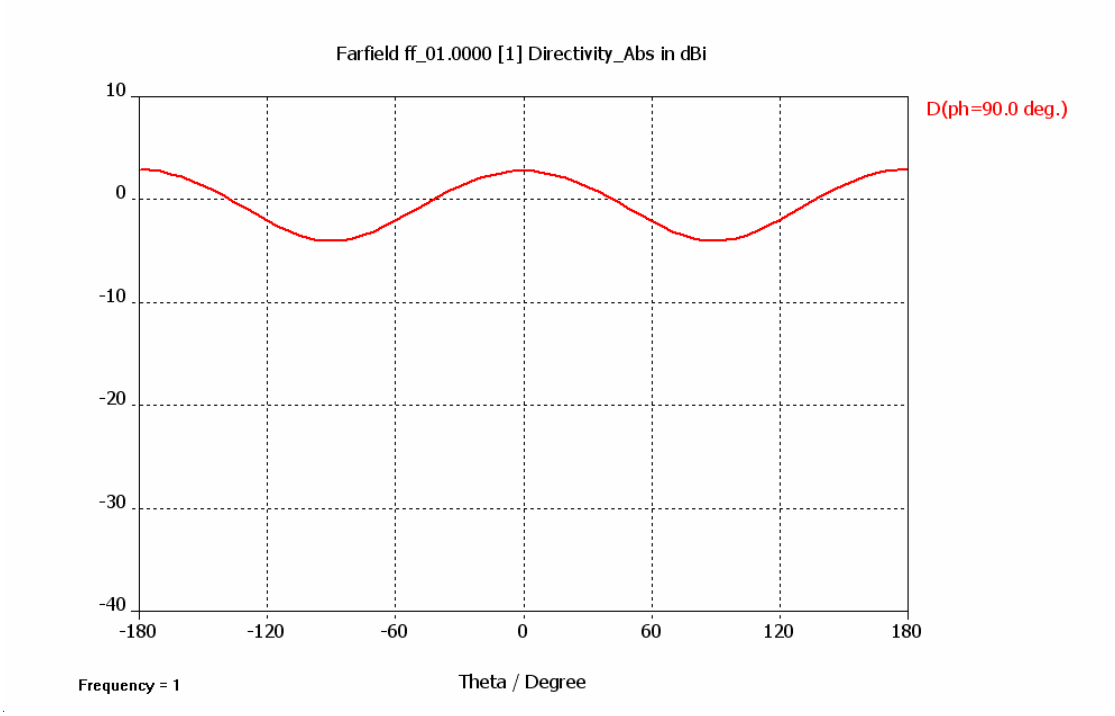

Figure 17. Plot showing the directivity of the antenna for $\phi = 90^o$ as predicted by Microwave Studio.

The radiation pattern is broad and bi-directional with equal beams radiated from the front and back of the structure, perpendicular to the plane of the antenna. The beam is circularly polarized on its axis over the usable bandwidth with the axial ratio rising slowly as the off-axis angle increases. Polarization is more sensitive to changes in frequency than is the pattern shape [37]. There is also no tilt to the lobe of the symmetrical antenna. By placing an absorbing material in a cavity behind the spiral antenna, the antenna exhibits a unidirectional radiation pattern. The disadvantage is that only half of the input power is transformed into radiated power because of the presence of the absorber. Morgan [34] considered the problem of achieving forward radiation from equiangular spiral antenna by rear loading.

Since the active region rotates at a rate dependent upon the spiral parameter as the frequency decreases, the radiation pattern would also rotate as the frequency decreases at the same rate. Hence, except for rotation, the radiation characteristics are ideally inde-

pendent of frequency [29]. The amount of rotation, $\Delta\phi$ (in radians), is given by the following equation

$$\Delta\phi = \frac{1}{a}\ln\left(\frac{f_1 + \Delta f}{f_1}\right), \tag{21}$$

where $a = 0.5$, $\Delta f = 0.5\,\text{GHz}$, giving $\Delta\phi = 46^o$. The amount of rotation is similar to the simulation as shown in Figures 18 and 19.

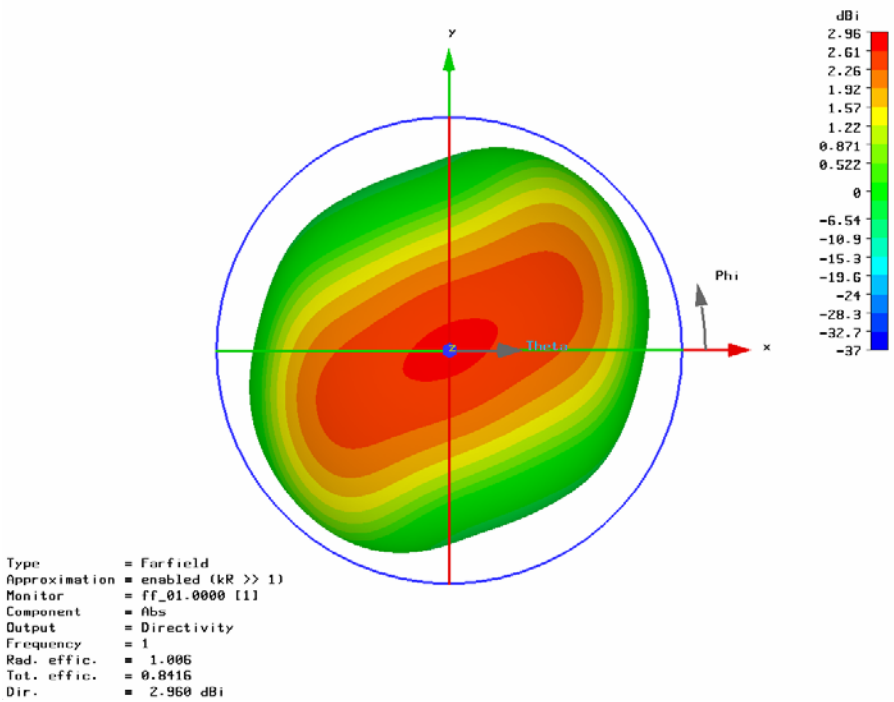

Figure 18. Plot showing the 3-D radiation pattern of the spiral antenna at 2 GHz.

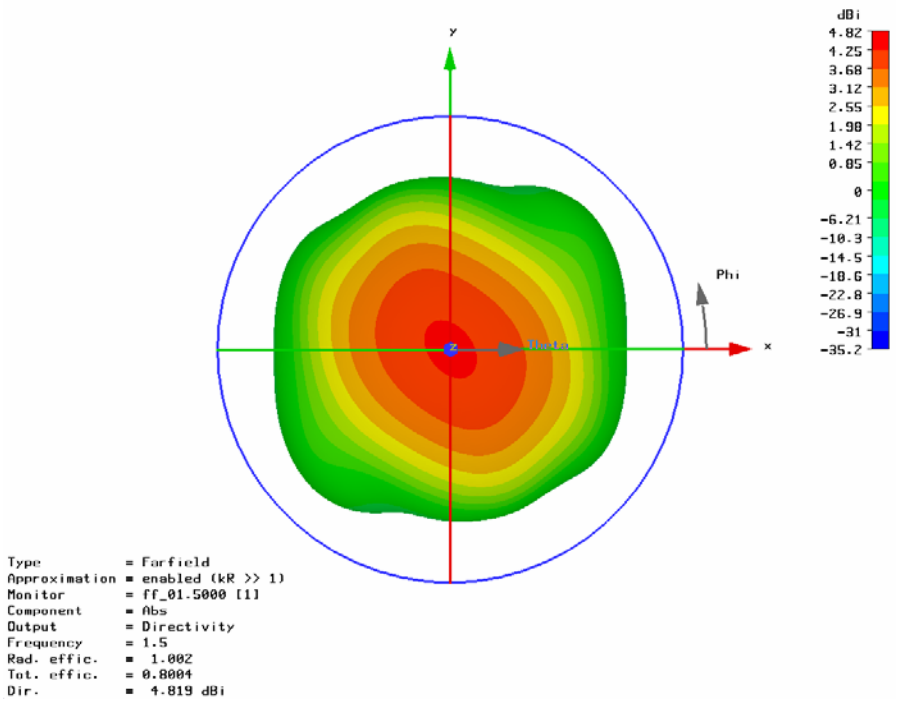

Figure 19. Plot showing the 3-D radiation pattern of the spiral antenna at 2.5 GHz.

The commonly used criterion for circular polarization requires that the axial ratio of the antenna be less than 6 dB [35]. The antenna axial ratio |AR| is defined as the ratio major axis electric field component to that along the minor axis. The sign of the axial ratio is positive for right-hand sense and negative for left-hand sense. Axial ratio is commonly expressed in decibels as 20log|AR|.

The idealized polarization of a right-handed spiral antenna for signal transmission and reception is shown in Figure 20. When used as a transmitting antenna, the radiation from the planar spiral antenna is right-hand circularly polarized (RHCP) in the forward direction (above) and left-hand circularly polarized (LHCP) in the backward direction (below). When used as a receiving antenna, the right-hand spiral antenna receives the right hand circularly polarized component (co-polarized component) of the electric field incident from the forward direction, while the left-hand circularly polarized component (the cross-polarized component) passes by the antenna mainly undetected. This circularly polarized field of the antenna can be beneficial when the antenna is used over the ground. Figure 21 shows the ratio of the electric fields of the LHCP and the RHCP components as a function of the angle of incidence [26]. Results are shown for dry, medium moist and

wet soils with the radar operating at frequency of 1.8 GHz. It is evident from the plot that the electric field of the reflected wave is predominantly cross-polarized to that of the incident wave, as long as the incident angle is not too large. Therefore, an ideal spiral antenna that radiates a LHCP wave towards the air/ground interface will not receive the wave reflected from the interface, because it is predominantly RHCP.

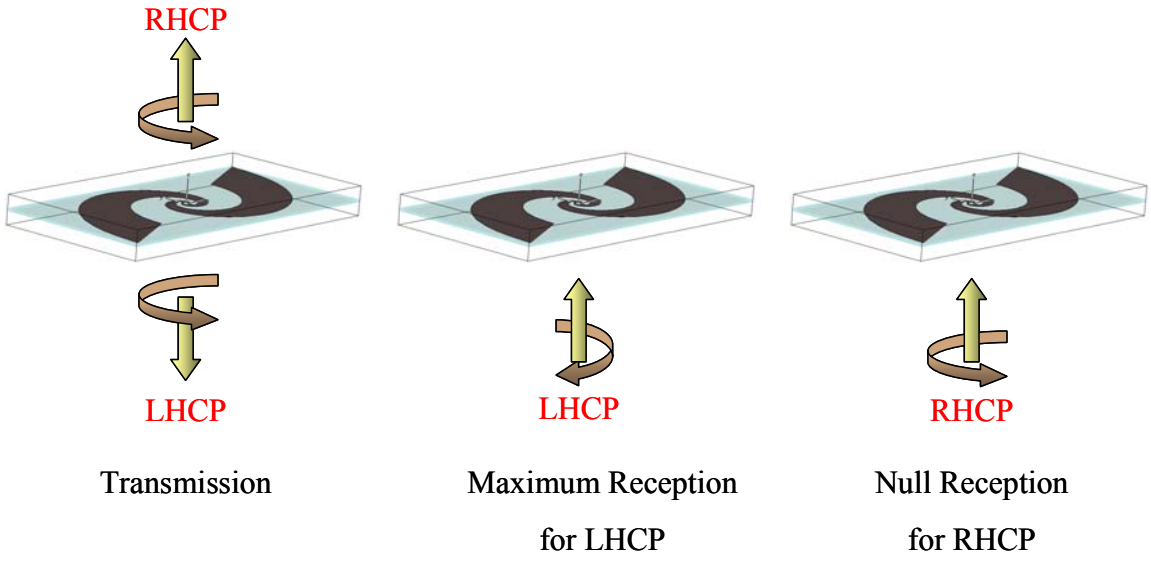

Figure 20. Idealized polarization characteristics of the right-handed spiral antenna.

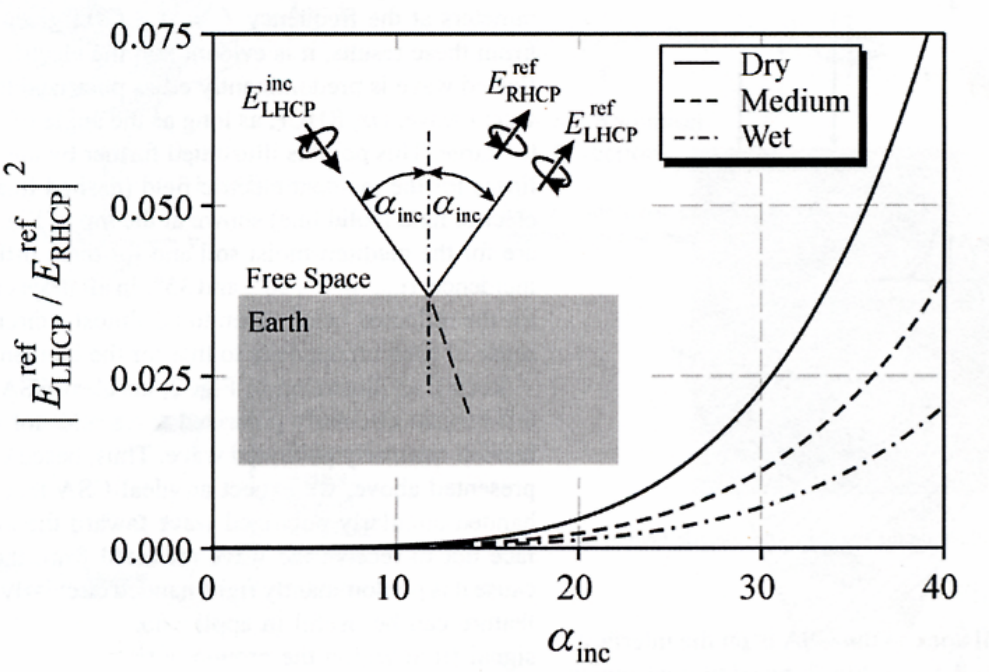

Figure 21. Ratio of *E*-fields of LHCP and RHCP waves as a function of the angle of incidence (From Ref. [26].).

The polarization of the radiated wave is determined by the length of the arms of the spiral antennas. Polarization is linear when the antenna arms are very short compared to one wavelength, and becomes elliptical as the frequency increases. For frequencies at which the arm lengths of the spiral antenna are greater than one wavelength, or slightly less, the polarization is circular and the input impedance remains almost constant as frequency varies [29, 35]. A typical variation in axial ratio of the on-axis field as a function of frequency for a one-turn slot antenna is shown in Figure 22 [29].

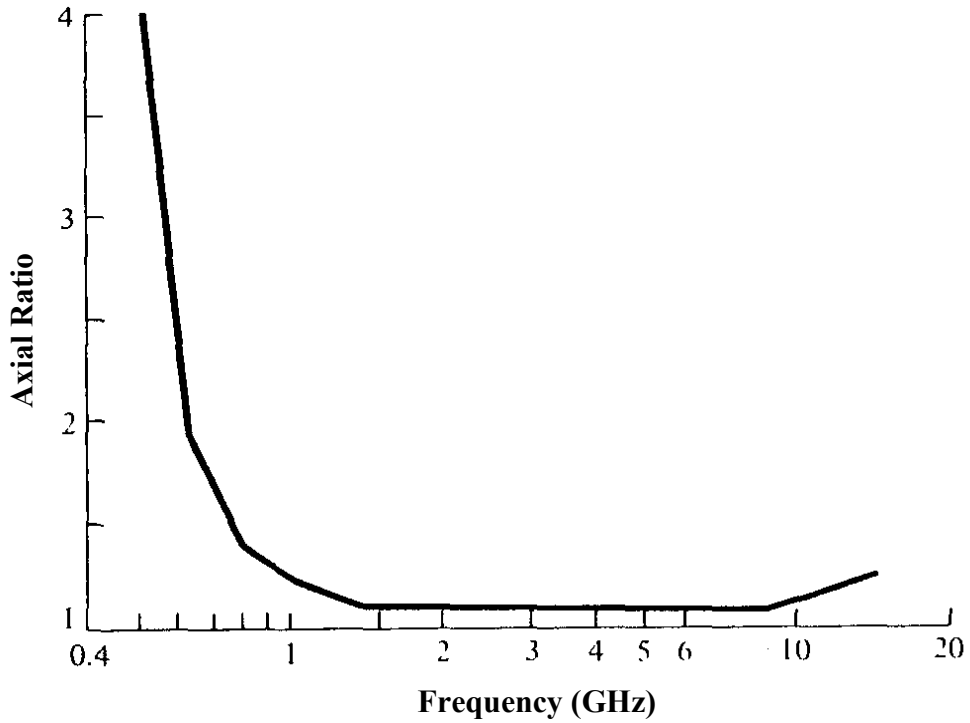

Figure 22. On-axis polarizations for one-turn spiral slot against frequency (From Ref. [29].).

The lowest frequency of operation is where the electrical length of the arm is one wavelength. The antenna simulated here has an arm length of 0.52 m, which results in an operating frequency of 0.58 GHz. The relationship between arm length and operating frequency of the spiral antenna is determined as follows.

The total length (L) of the spiral arm can be calculated by

$$L = \int_{\rho_0}^{\rho_1} \left[\left(\rho^2 \frac{d\phi}{d\rho} \right)^2 + 1 \right]^{1/2} d\rho , \tag{22}$$

$$L = (\rho_1 - \rho_0) \sqrt{1 + \frac{1}{a^2}} , \tag{23}$$

where ρ_0 and ρ_1 refer to the inner and outer radii of the spiral antenna, and $a = 0.5\,\text{rad}^{-1}$ is the growth rate of the spiral. Substituting $\rho_o = 0.0021$ m and $\rho_1 = 0.233767$ m gives the

spiral antenna arm length as 0.52 m, which results in the lowest operating frequency of 0.58 GHz. Figure 22 shows the variation of the antenna on-axis polarization with frequency for the spiral antenna designed.

It can be concluded from the axial ratio plots (Figures 23 to 27) that the spiral antenna is circularly polarized in the $\theta = 0°$ direction for the frequencies simulated. Circular polarization is expected at frequencies up to the acceptable S_{11} parameter. At this limit, the size of the feed region becomes small compared to the feed input.

Figure 28 shows the return loss (the magnitude of the S_{11}-parameter in dB) of the planar spiral antenna in the frequency range from 1 to 6 GHz. The return loss was found to be better than -10 dB from 1 to about 5 GHz. The Smith chart normalized to the input impedance of 140 Ω is also shown in Figure 29.

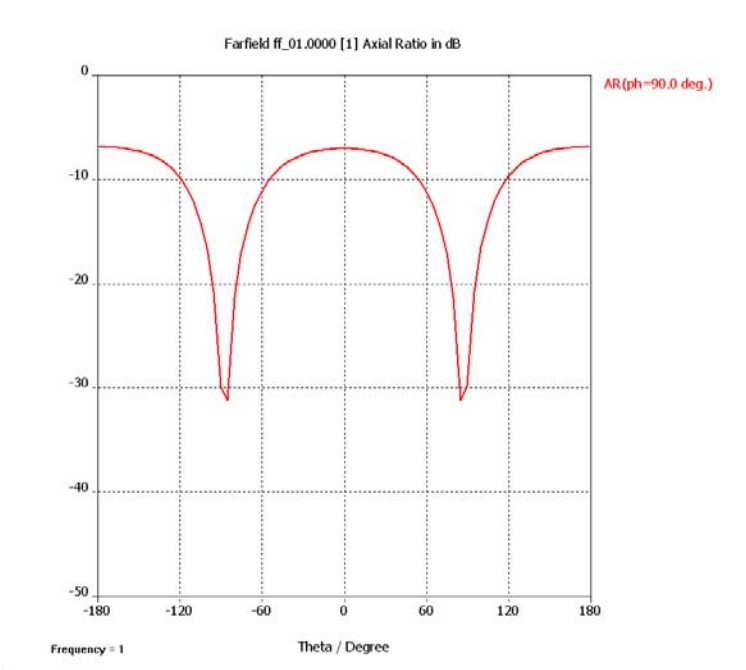

Figure 23. Axial ratio of the spiral antenna at frequency f = 1 GHz.

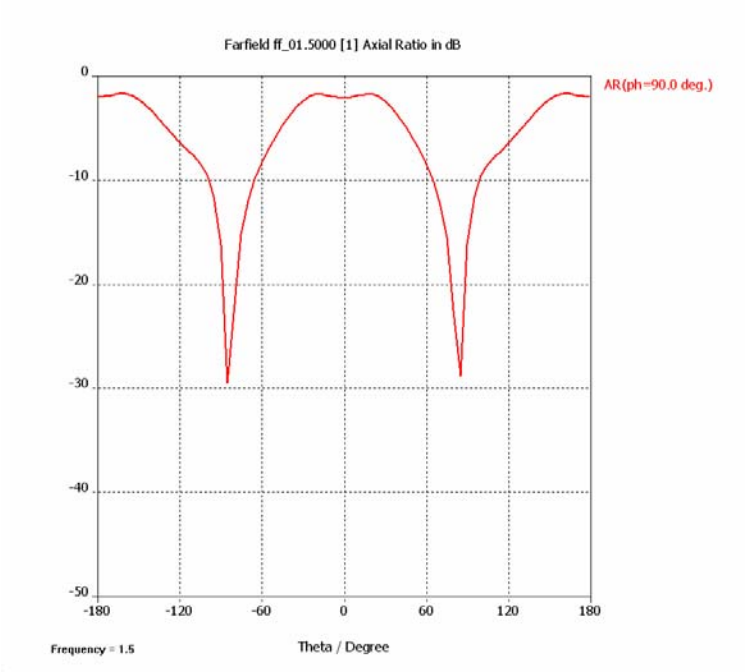

Figure 24. Axial ratio of the spiral antenna at frequency f = 1.5 GHz.

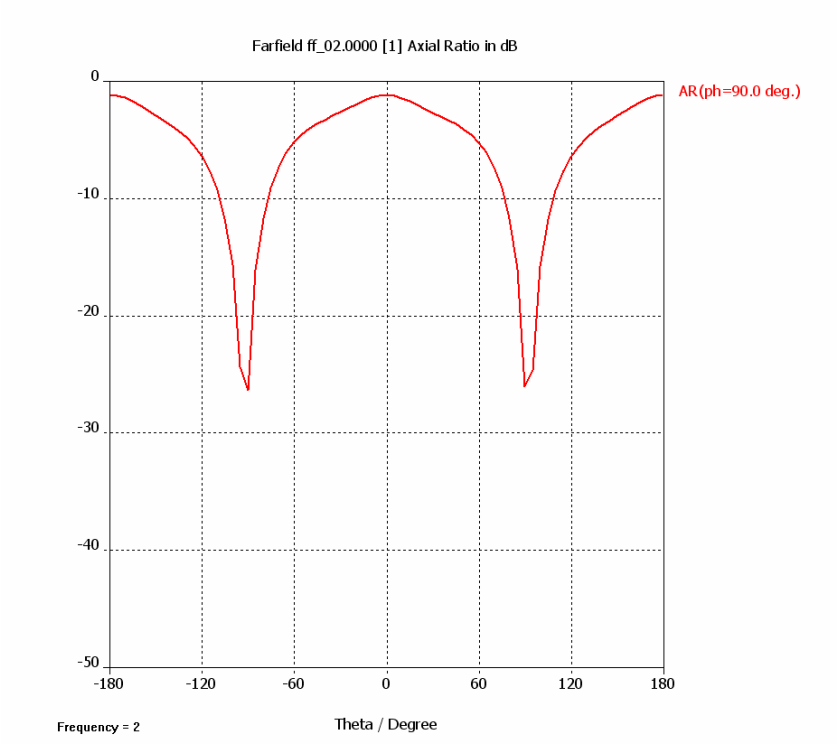

Figure 25. Axial ratio of the spiral antenna at frequency f = 2 GHz.

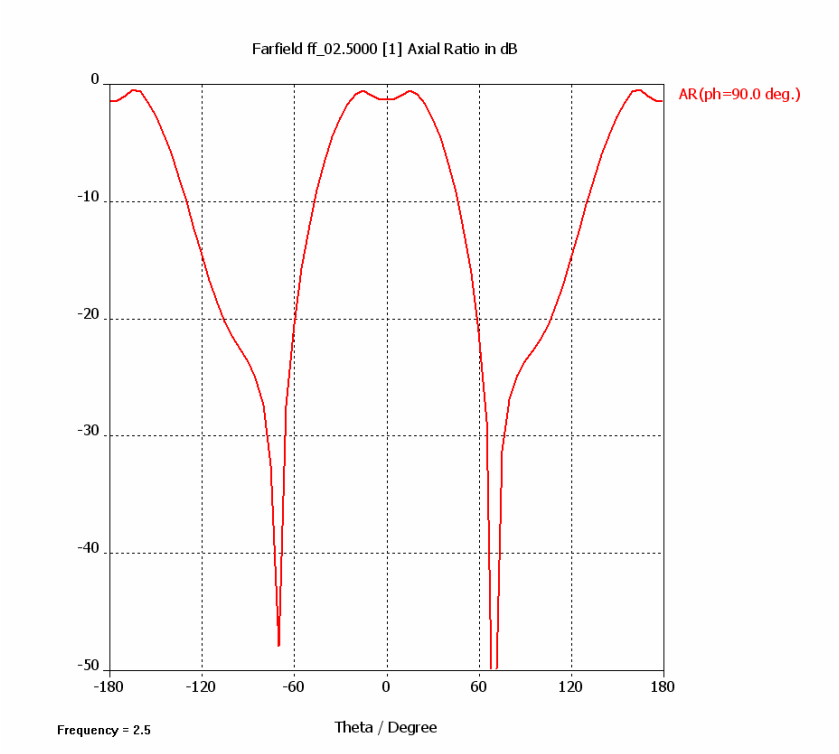

Figure 26. Axial ratio of the spiral antenna at frequency $f = 2.5$ GHz.

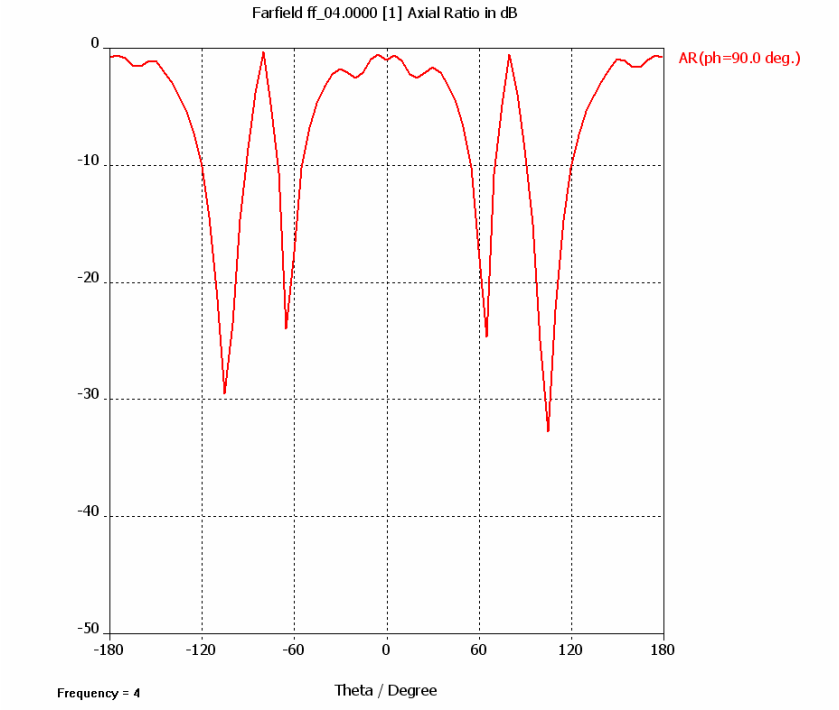

Figure 27. Axial ratio of the spiral antenna at frequency $f = 4$ GHz.

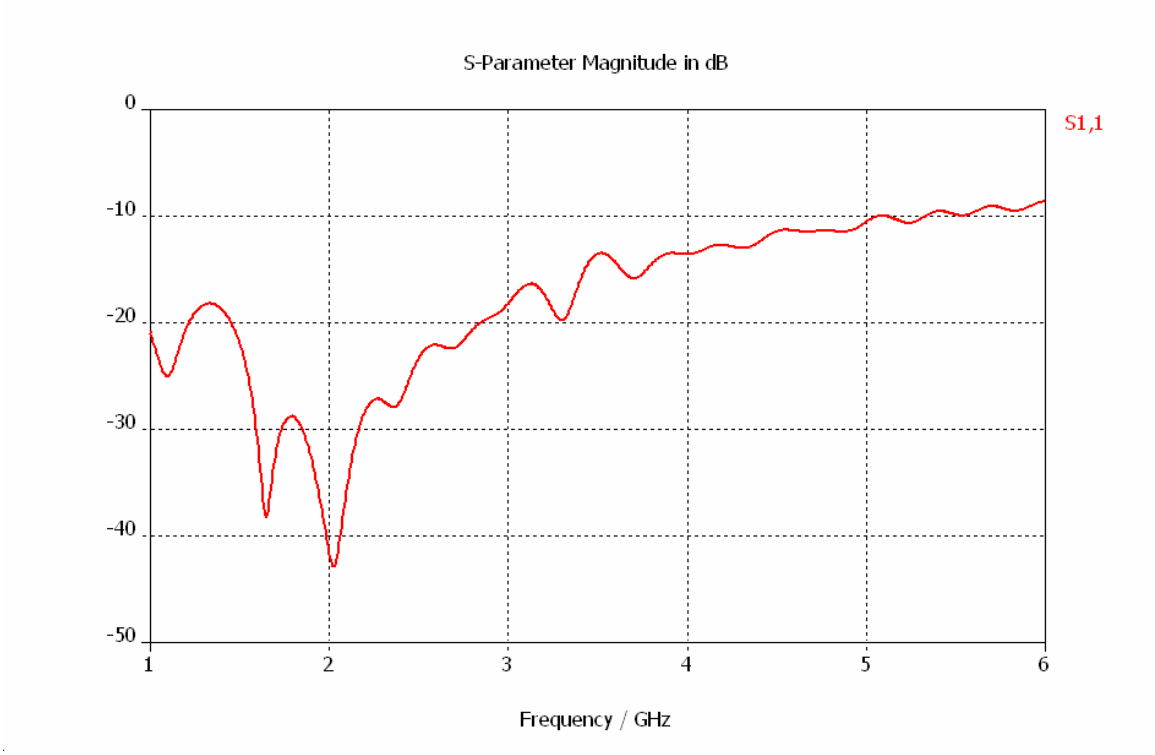

Figure 28. Return loss for planar spiral antenna.

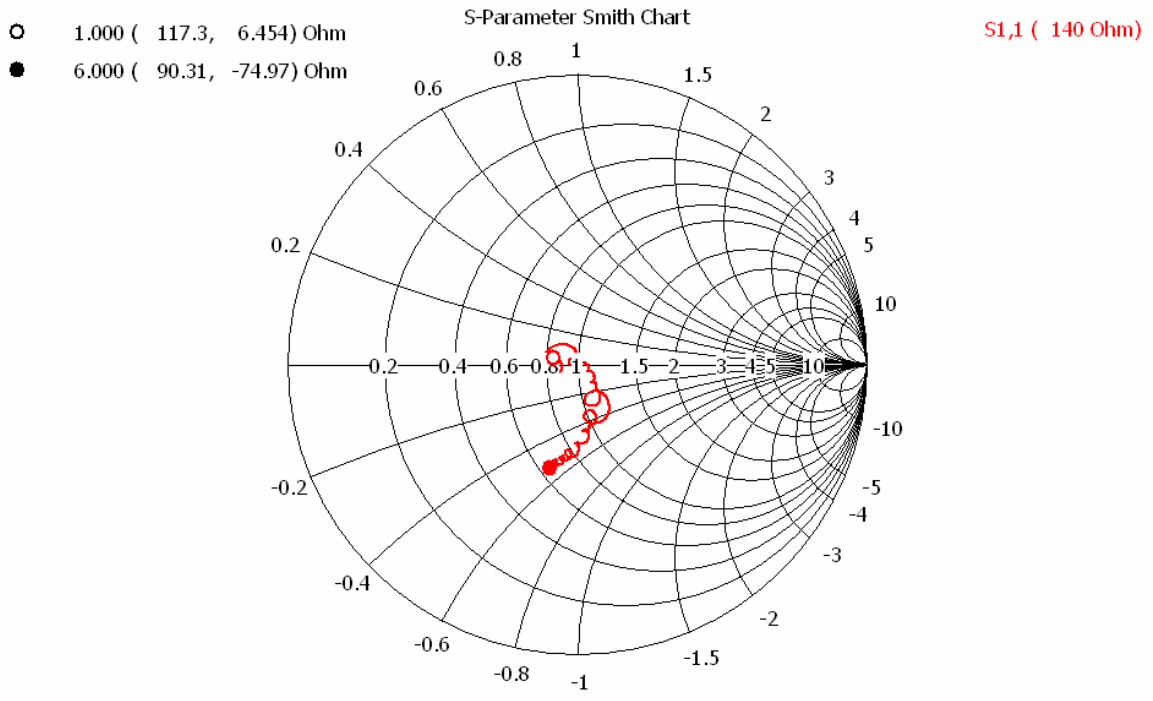

Figure 29. Smith chart plot of planar spiral antenna impedance normalized to 140 Ω.

Thaysen [33] has also observed that there is very little difference in the S_{11}-parameter for the spiral antenna with or without a cavity. The bandwidth of the antennas is often defined by the range of the frequencies that mark the bounds of acceptable performance. The above antenna design has a bandwidth of approximately 5 GHz.

The equiangular spiral antenna described is a balanced antenna and requires a balun to transform the unbalanced coplanar waveguide (CPW) feed line to a balanced coplanar strip (CPS) feed line for input to the spiral antenna. The bandwidth of the system is limited by the balun when an electrically unbalanced feed line is used [37]. Thaysen [38] presented a design for a wideband balun to accomplish the transition from the unbalanced CPW to the balanced CPS transmission line. The balun has insertion loss of less than 3 dB from 100 kHz and up to a frequency of 3.85 GHz. A four-section Chebyshev impedance transformer was designed in order to transform the impedance from 50 ohms to the spiral antenna impedance of 80 ohms. The reflection coefficient was found to be less than 5 dB.

Simulations of spiral antennas placed on substrates of different relative permittivity have shown that the impedance of the antenna decreases with increased permittivity. Figure 30 shows that the input impedance of the antenna for a substrate permittivity of 1.06 is 200 Ω at 2 GHz.

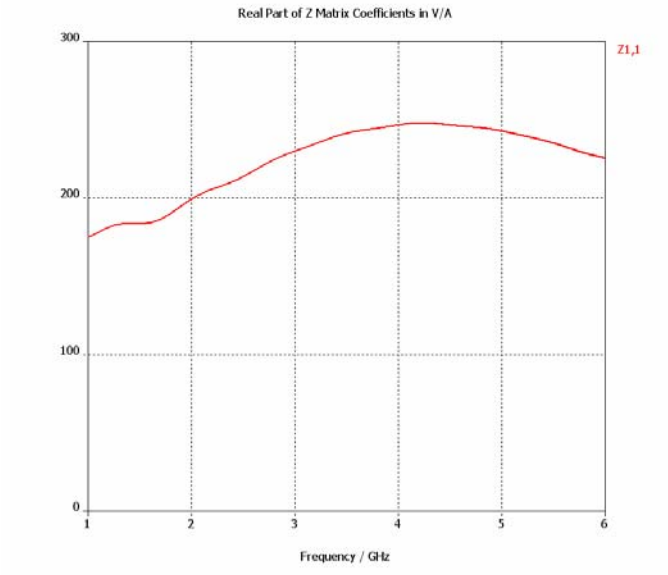

Figure 30. Variation of input resistance with frequency for ε_r=1.06.

C. SUMMARY

A frequency-independent antenna is one whose radiation pattern, impedance and polarization remain virtually unchanged over a large bandwidth. The design of a frequency-independent antenna is based upon the fundamental principle that, if the shape of the antenna were such that it could be specified entirely by angles, its performance would be independent of frequency.

The planar spiral antennas have useful properties for subsurface applications. The polarization of the radiated wave from the planar spiral is determined by the length of the arms of the spiral antennas. For frequencies where the arm lengths of the spiral antenna are greater than one wavelength, the polarization is circular and the input impedance remains almost constant as frequency varies. The impedance of the antenna decreases with increased substrate permittivity.

The counter-wound spiral antenna (CWSA) design examined in the next chapter aims to minimize losses due to polarization mismatch between the scattered fields from the subsurface and the receiving antenna. When the scattered field from the buried objects or interface is linearly polarized, the use of a circularly polarized receiving antenna would result in 3-dB polarization loss.

IV. COUNTER-WOUND SPIRAL ANTENNA DESIGN

As mentioned in Chapter III, the ideal equiangular spiral antenna will not receive waves reflected from the air/ground interface because the electric field (*E*-field) of the reflected wave is predominantly cross-polarized to that of the incident wave, as long as the incident angle is not too large.

The RCS of a target depends on many factors such as the frequency and polarization of the incident wave, as well as the target material and target aspect [39]. Target aspect refers to the orientation of the target with respect to the *E*-field of the incident wave.

The polarization of a uniform plane wave describes the shape and locus of the tip of the *E*-field vector in the plane orthogonal to the direction of propagation, at a given point in space as a function of time. Figure 31 [40] shows a snapshot of a plane wave propagating in the +*y*-direction at a fixed instant of time. The wave is linearly polarized since the *E*-field at a fixed point oscillates up and down along a vertical line in the *z*-direction.

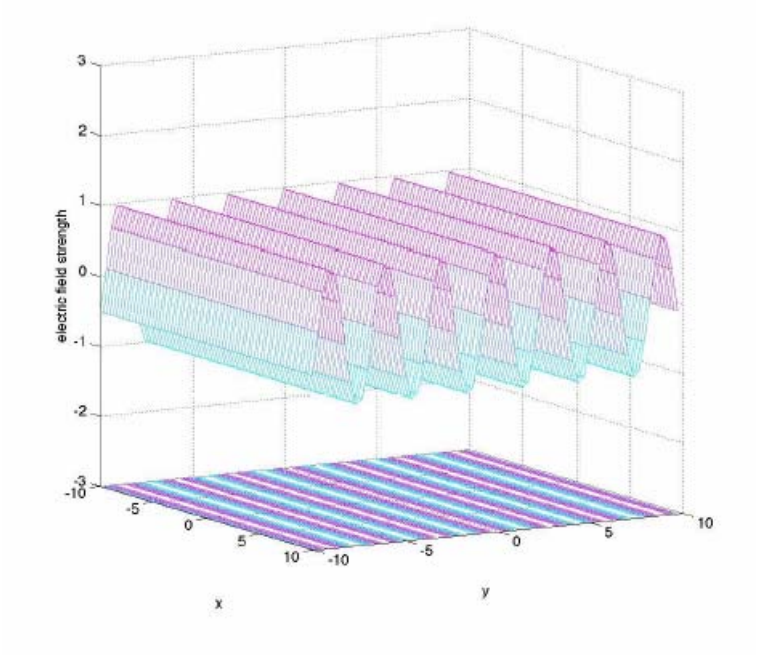

Figure 31. Spatial variation of E-field at $t = 0$ for the plane wave propagating in +*y*-direction (From Ref. [40].).

For a plane wave propagating in the *z*-direction, the *z*-components of both the electric and magnetic fields are zero. The E-field of a time-harmonic wave may be described by phasors (denoted by ~)

$$\widetilde{E}(z) = \hat{x}\widetilde{E}_x(z) + \hat{y}\widetilde{E}_y(z) \tag{24}$$

with

$$\widetilde{E}_x(z) = E_{x0}e^{-jkz} \tag{25a}$$

$$\widetilde{E}_y(z) = E_{y0}e^{-jkz}e^{j\delta}, \tag{25b}$$

where E_{x0} and E_{y0} are the amplitudes of the components of $\widetilde{E}_x(z)$ and $\widetilde{E}_y(z)$, respectively. The phase of a wave is defined relative to a reference condition with specified values of *z* and *t*. The wave polarization depends on the relative phase of $\tilde{E}_x$ with respect to $\tilde{E}_y$, not their absolute phases.

For a linearly polarized wave, the *E*-field at a fixed point oscillates back and forth along a line, that is, the $E_x(z,t)$ and $E_x(z,t)$ components are either in phase or out of phase ($\delta = 0, \pi$). For a circularly polarized wave, the components of the *E*-fields, $E_x(z,t)$ and $E_y(z,t)$ remain constant and the phase difference between the fields is 90 degrees ($\delta = \pm\pi/2$). Hence, a circularly polarized wave can be obtained by superimposing two equal-amplitude linearly polarized plane waves that are in space and time quadrature.

The sense of the polarization is defined in terms of the rotation of the *E*-field as a function of the time in a fixed plane orthogonal to the direction of propagation, which is opposite of the direction of rotation of *E*-field as a function of distance at a fixed point in time. The designation of RHCP is determined by the right-hand rule and LHCP by the left-hand rule. Figure 32 shows RHCP and LHCP waves.

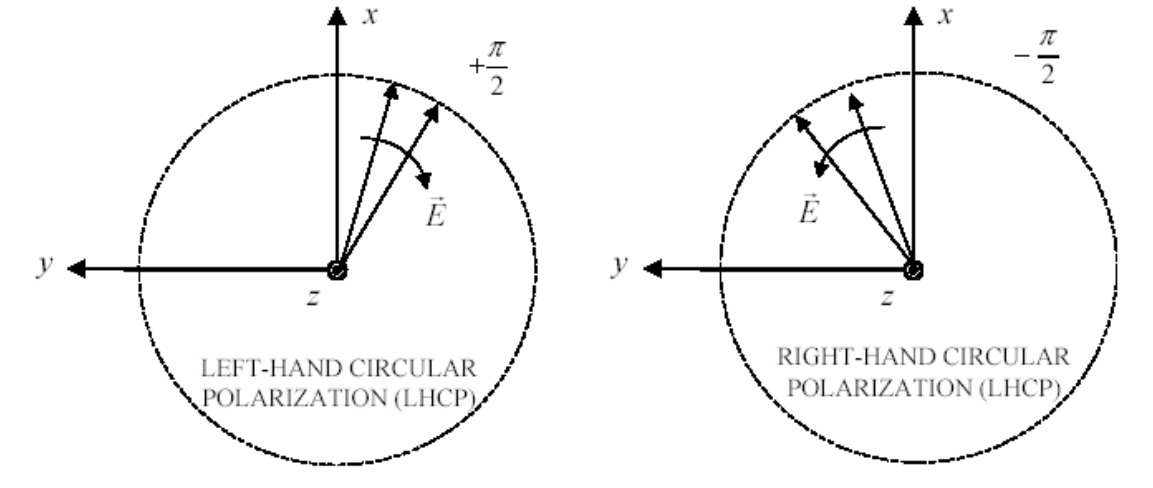

Figure 32. *E*-field variations of the RHCP and the LHCP waves (From Ref. [40].).

Polarization efficiency is given by the polarization mismatch factor, *p*. It is used to determine the polarization mismatch between the received wave and the antenna. The polarization efficiency varies from a minimum of 0 to a maximum of 1 as the incoming wave and the receiving antenna vary from a completely mismatched to a completely matched condition. A complete match ($p = 1$) exists when the wave and the antenna polarization states are exactly identical, which will result in maximum antenna output voltage. A complete mismatch of the system ($p = 0$) occurs when the wave and antenna are cross-polarized, which will result in a null output. Orthogonal linear states such as horizontal and vertical linear polarization (LP) and right-hand and left-hand circular polarizations (CP) are examples of cross-polarized states.

The polarization of the scattered field is not necessarily the same as that of the incident field. Most targets will generate cross-polarized scattering components due to multiple reflections and diffractions arising from the nature of the objects. A scattering matrix can be used to completely specify the relationship between the incident and the scattered fields

$$\begin{bmatrix} E_{s\theta} \\ E_{s\phi} \end{bmatrix} = \begin{bmatrix} S_{\theta\theta} & S_{\theta\phi} \\ S_{\phi\theta} & S_{\phi\phi} \end{bmatrix} \begin{bmatrix} E_{i\theta} \\ E_{i\phi} \end{bmatrix} \tag{26}$$

where $\{S_{pq}\}$ are the scattering parameters, and p and q can be either θ or ϕ. The first parameter specifies the polarization of the receive antenna and the second the polarization of the wave. The elements of the scattering matrix are complex quantities.

One half of the power available from a LP wave is lost when received by a CP antenna. The LP wave can be decomposed into equal components of RHCP and LHCP waves. If the receiving antenna is circularly polarized, it will only be receiving either one of the components, since the other one will be co-polarized. The same is true for a CP wave and an LP antenna. In most applications, this 3-dB loss is significant and hence a receiving antenna that is matched to the polarization of the incoming wave must be used.

Thus, for an antenna to be able to detect a buried object, the scattered electric field from the object must contain a significant co-polarized component. For a buried perfectly conducting thin rod shown in Figure 33, the scattered field from a thin rod will be linearly polarized, and its field can be decomposed into equal LHCP and RHCP components. For the spiral antenna shown, only half of the backscattered power will be received by the antenna, reducing the probability of target detection.

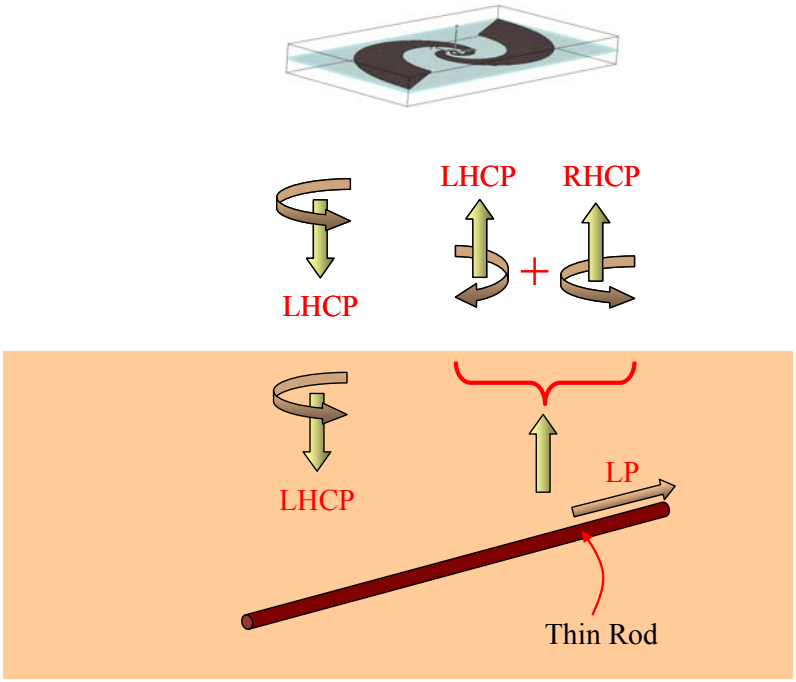

Figure 33. Geometry of a monostatic GPR that uses a single spiral antenna to detect thin rods buried in the ground.

A. COUNTER-WOUND SPIRAL ANTENNAS IN FREE SPACE

The counter-wound spiral antenna (CWSA) design examined here aims to minimize losses due to polarization mismatch between the scattered fields from the subsurface and the receiving antenna. This is achieved by having two sets of dual-arm spiral antennas, counter-wound and stacked over each other along the antenna main axis as shown in Figure 34. The design of each of the planar duo-arm equiangular-spiral antennas was based on the same fundamental design principles discussed in Chapter III. The two planar antennas can be fabricated on separate sides of the same substrate, with the substrate thickness determining the spacing between the two spirals.

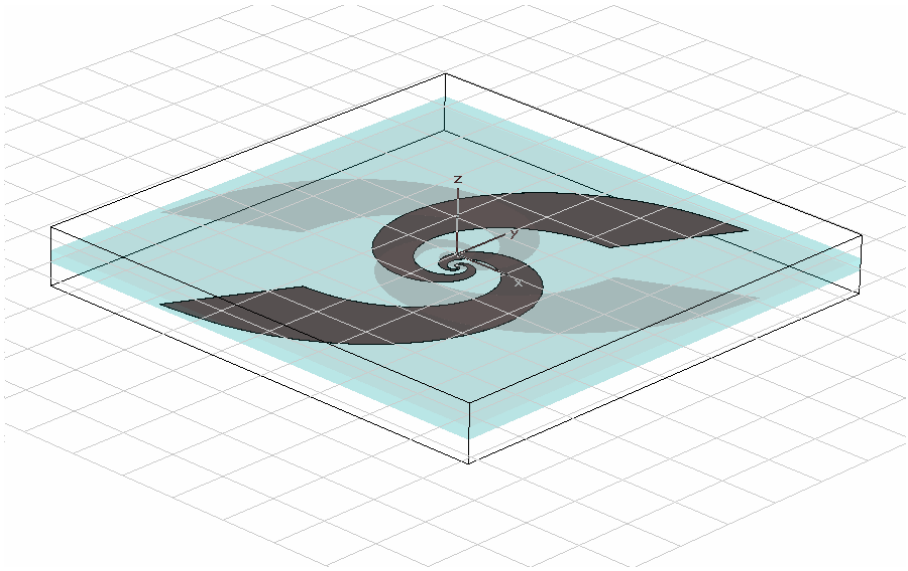

Figure 34. Geometry of a counter-wound spiral antenna.

The objective of the design is to achieve an antenna radiation pattern and impedance that remains virtually unchanged over a large bandwidth. With the CWSA, the polarization of the wave transmitted by the antenna can be made linear, either vertically or horizontally polarized, by varying the delays to the signals that are being sent to the antenna feeds of the spirals. This design allows the buried objects to be radiated by both vertically and horizontally polarized waves, reducing the polarization loss in the received scattered signal from the subsurface objects, thereby allowing better detection of targets which may lie in any arbitrary orientation with respect to the main antenna axis.

Although the linearly polarized wave will receive reflections from the ground, they can be removed by signal processing, using delay line cancellers or other techniques commonly used in today's airborne radar systems. Peter [41] has successfully achieved greater than 30 dB of clutter suppression by subtracting the extraneous clutter (without the target) coherently from the data collected with the desired target present. This signal-to-clutter ratio (SCR) was further enhanced by using high range resolution processing.

The performance of several CWSAs was determined through simulation for different separations and orientations between the two planar spiral antennas. The resultant polarization of the CWSA was also determined by calculating the axial ratio of the *E*-fields at different distances and displacements from the antenna axis. The frequency-independent characteristics of the antenna, like its impedance and radiation patterns over a wide bandwidth, are also determined through software simulation. The results of the simulations for different parameters in the antenna design are shown in the following subsections.

When both antennas are transmitting, the combined signal will be linearly polarized under ideal conditions, that is, when the two spirals lie very close together and yet do not interfere with each other. Similarly, on receiving, the combined output of the two spirals will be linearly polarized.

As shown in Figure 35, the top spiral arms, which have a bi-directional radiation pattern, will transmit a LHCP wave to the rear counter-wound spiral antenna. Ideally the wave should pass through the rear antenna because it has the opposite polarization sense. The addition of the *E*-fields from the top antenna (RHCP) and the rear antenna (LHCP) will result in a linearly polarized wave in the forward direction.

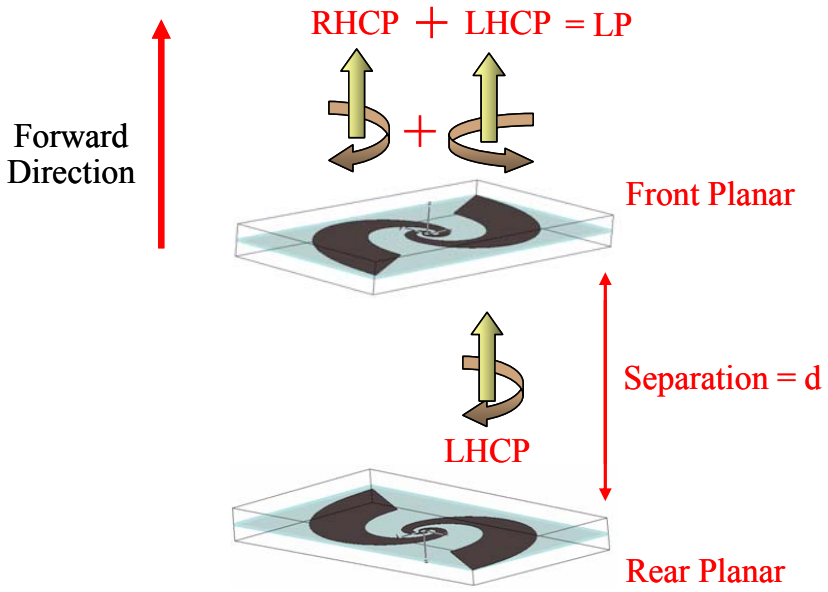

Figure 35. Setup for determining the reflection coefficients of the counter-wound spiral antenna.

Figure 36 shows the S_{11}-parameter of the top planar spiral antenna for a substrate thickness of 20 mm, for frequencies ranging from 1 to 6 GHz, with the rear antenna feed terminated in a resistive load equal to the estimated antenna impedance of 140 Ω. This condition gives an indication of the coupling or interference presented by the bottom antenna to the top antenna. The S_{11}-parameter of the antenna was found to be better than -10 dB from 1 GHz to 3.8 GHz. The subsurface radar can then be designed to operate in this frequency band for low reflection coefficients. The Smith chart normalized to an impedance of 140Ω is also shown in Figure 37. For this setup, the top and rear spiral arms are rotated at 90 degrees as shown in Figure 34.

It can be seen from these plots that an operating bandwidth of about 3.8 GHz is possible for an antenna separation of 20 mm. Figures 38 and 39 shows the simulation results for a substrate thickness of 30 mm. It is concluded from the plots that a substrate thickness of 30 mm is required to achieve a continuous bandwidth of about 4.8 GHz (based on S_{11} alone) when the counter-wound spiral antennas are setup as in Figure 34.

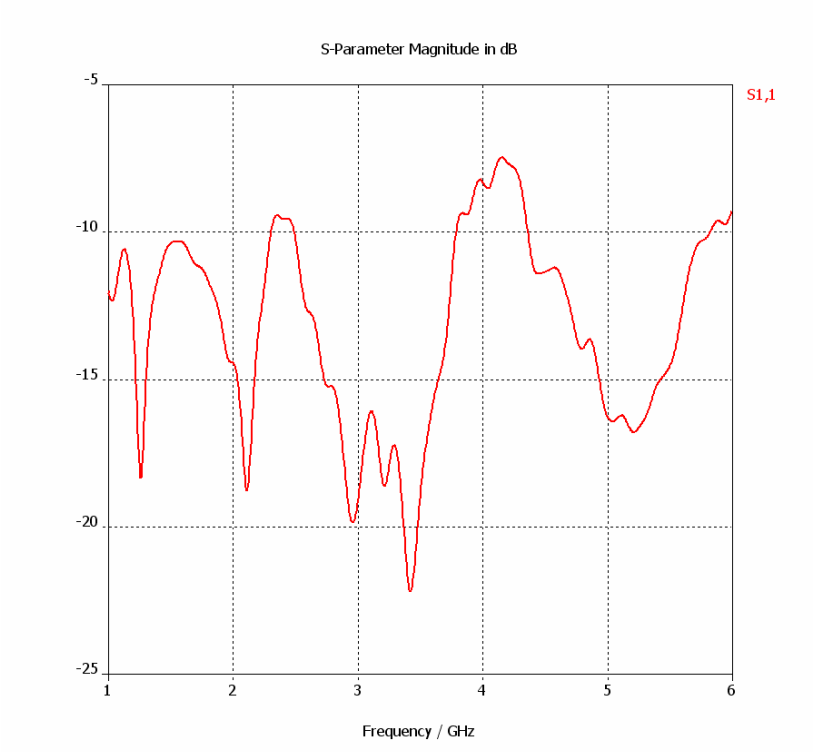

Figure 36. Return loss of the CWSA with substrate thickness of 20 mm.

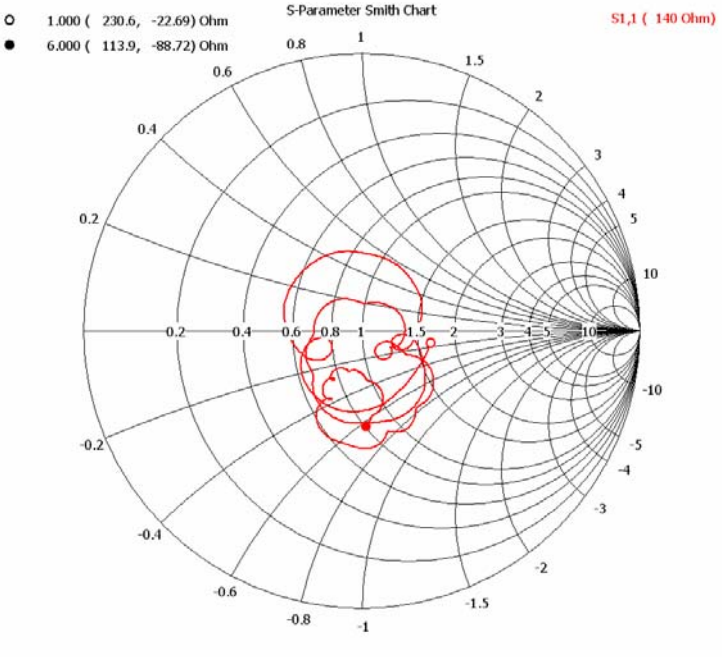

Figure 37. Smith chart for the CWSA with substrate thickness of 20 mm.

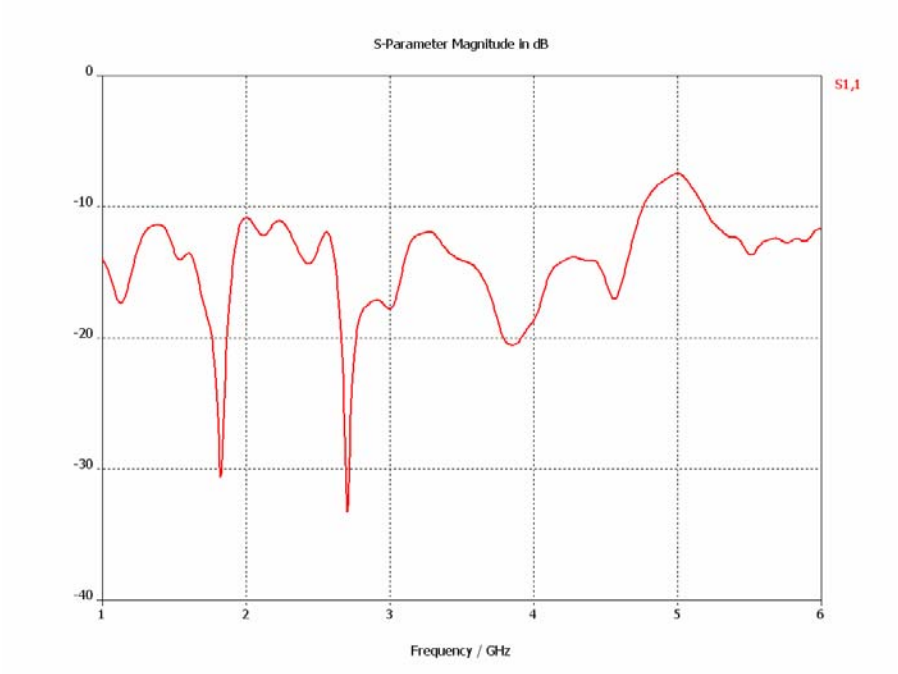

Figure 38. Return loss of the CWSA with substrate thickness of 30 mm.

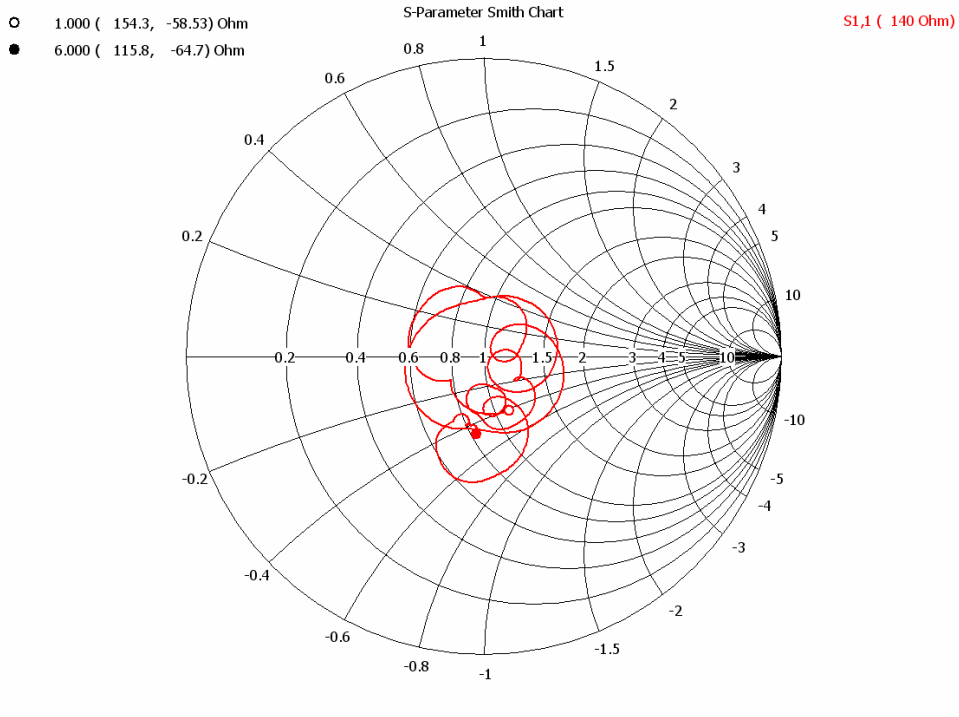

Figure 39. Smith chart for the CWSA with substrate thickness of 30 mm.

Simulation has also been performed to determine the performance of the CWSA design as shown in Figure 40. In this design, the spiral arms are counter-wound, but are not rotated 90 degrees to each other as in the previous case. Simulations were performed to determine the return loss of the un-rotated CWSA for a substrate thickness of 100 mm, for frequencies ranging from 1 to 6 GHz. The rear antenna feed was also terminated with a resistive load value equal to the estimated impedance of the spiral antenna.

The return loss and Smith chart of the un-rotated CWSA are as shown in Figures 41 and 42. It can be concluded from the plots that a substantial increase in the separations between the planar spirals is required in order to achieve similar performance to that of the rotated case. This un-rotated design allows a smaller overall antenna footprint but at the expense of a much wider separation between the spiral arms.

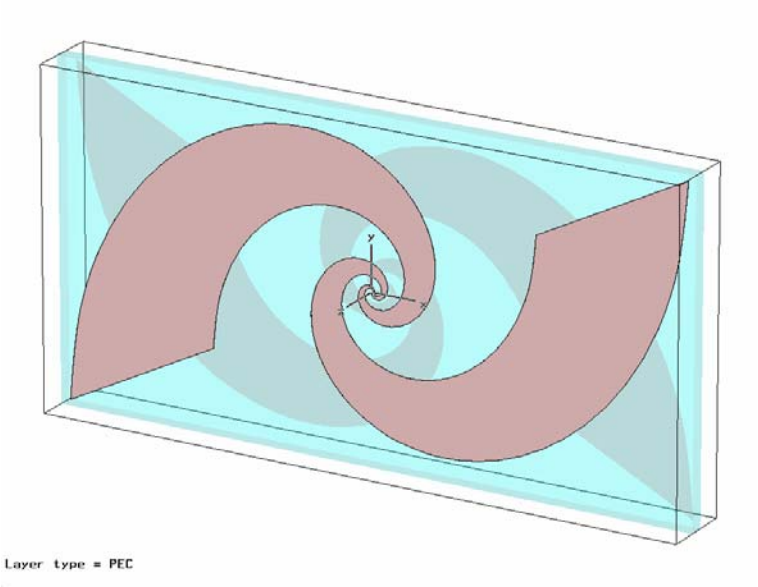

Figure 40. Geometry of an un-rotated counter-wound spiral antenna.

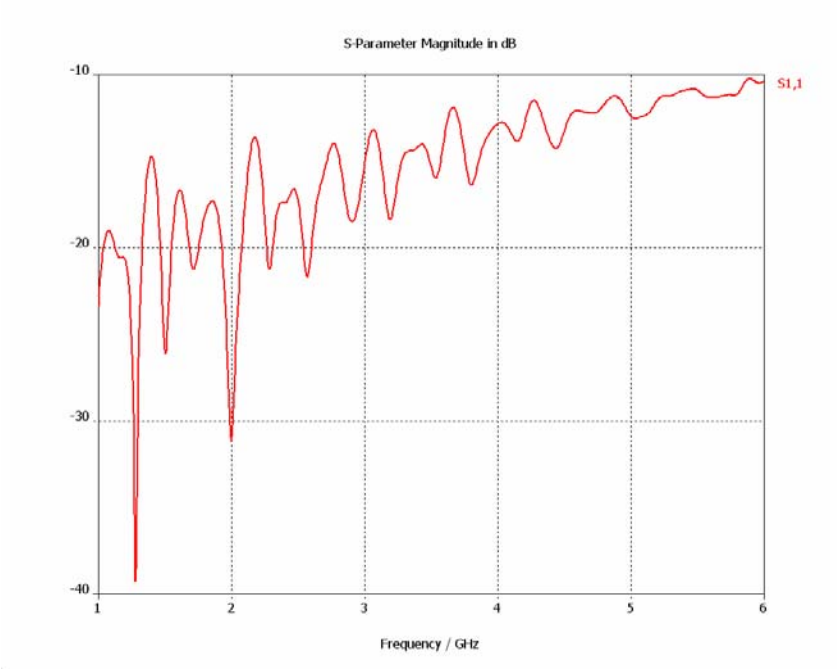

Figure 41. Return loss of the un-rotated CWSA with substrate thickness of 100 mm.

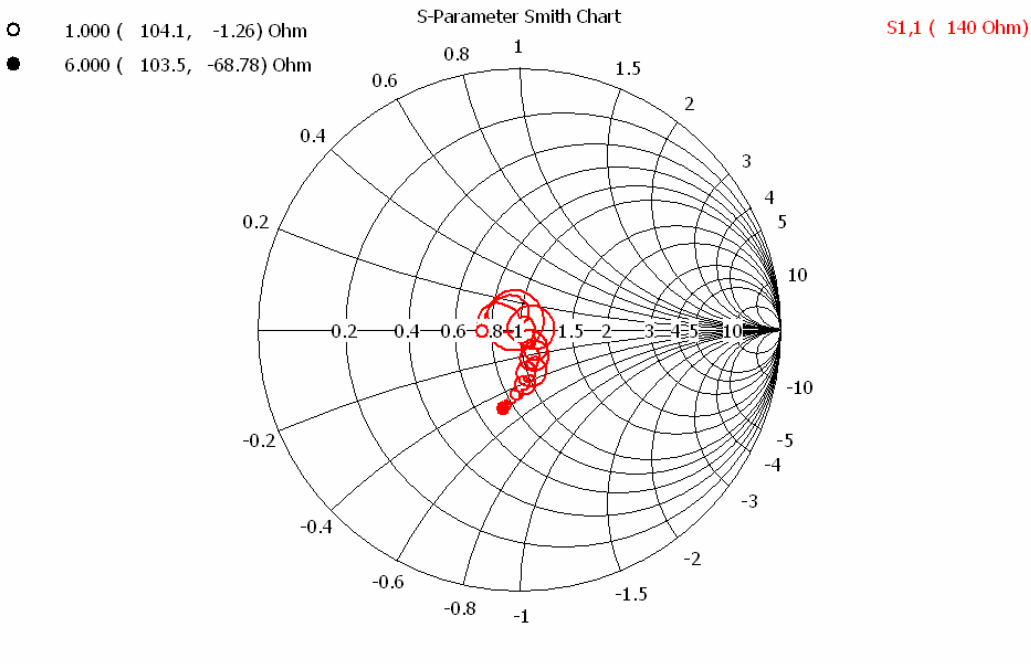

Figure 42. Smith chart for the un-rotated CWSA with substrate thickness of 100 mm.

The polarization when both planar duo spiral arms are simultaneously excited is shown in Figure 43. The *E*-field of the RHCP wave radiated by the front planar spiral is being added to the *E*-field of the LHCP wave transmitted by the counter-wound rear spiral. The resultant polarization of the CWSA would be a linearly polarized wave traveling in the forward direction towards the ground.

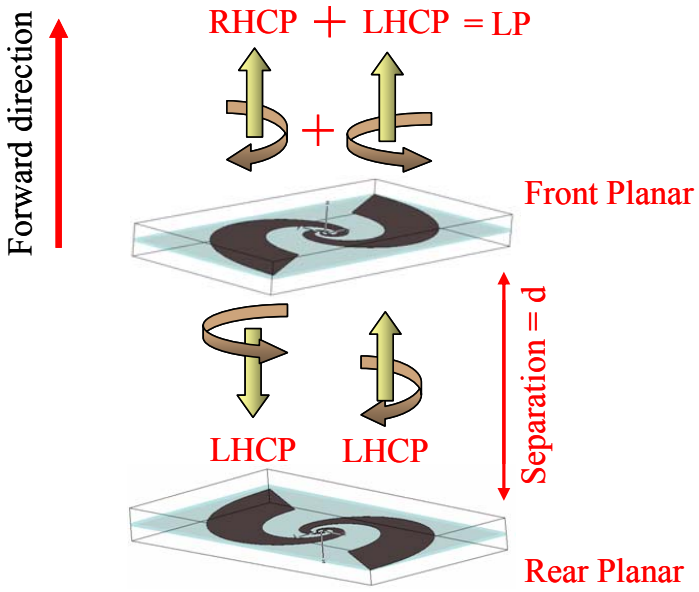

Figure 43. Linear polarization from a counter-wound spiral antenna.

The linear polarization can be shown mathematically as follows. The *E*-field of a RHCP wave can be represented as a vector given by

$$\vec{E}_{RHCP} = E_o(\hat{x} - j\hat{y})e^{-jk\left(z-\frac{d}{2}\right)}, \tag{27}$$

and the *E*-field of a LHCP wave represented by

$$\vec{E}_{LHCP} = E_o(\hat{x} + j\hat{y})e^{-jk\left(z+\frac{d}{2}\right)}e^{j\phi} \tag{28}$$

where $\hat{x}$ and $\hat{y}$ are the unit vectors in the *x* and *y* directions respectively. The separation between the front and rear spiral antennas is given by *d*, and $e^{j\phi}$ is an arbitrary phase difference between the front and rear antennas. This is illustrated in Figure 43.

For an observation point at z, the resultant E-field due to the addition of the RHCP and LHCP waves is given by

$$\begin{aligned}\vec{E}_{TOT} &= E_0 e^{-jkz}\left[\hat{x}\left(e^{jk\frac{d}{2}}+e^{-jk\frac{d}{2}}e^{j\phi}\right)+\hat{y}\left(e^{jk\frac{d}{2}-j\frac{\pi}{2}}+e^{-jk\frac{d}{2}+j\frac{\pi}{2}}e^{j\phi}\right)\right],\\ &= E_0 e^{-jkz}\left[\hat{x}e^{j\frac{\phi}{2}}\left(e^{jk\frac{d}{2}-j\frac{\phi}{2}}+e^{-jk\frac{d}{2}+j\frac{\phi}{2}}\right)+\hat{y}e^{j\frac{\phi}{2}}\left(e^{jk\frac{d}{2}-j\frac{\pi}{2}-j\frac{\phi}{2}}+e^{-jk\frac{d}{2}+j\frac{\pi}{2}}\right)\right], \qquad (29)\\ &= 2E_0 e^{-jkz}e^{j\frac{\phi}{2}}\left[\hat{x}\cos\left(\frac{kd}{2}+\frac{\phi}{2}\right)+\hat{y}\sin\left(\frac{kd}{2}+\frac{\phi}{2}\right)\right],\end{aligned}$$

which is a linearly polarized wave with its electric field vector rotated from the x-axis by an angle α where

$$\tan\alpha = \tan\left(\frac{kd}{2}+\frac{\phi}{2}\right). \qquad (30)$$

A phase difference $\phi = 180°$ between the front and rear antennas will result in a rotation of the resultant field $\vec{E}_{TOT}$ by $90°$. For the case of $d = 0$ and $\phi = 0°$,

$$\vec{E}_{TOT} = 2E_0 e^{-jkz}\hat{x}, \qquad (31)$$

which is a horizontally polarized wave. For the case of $d = 0$ and $\phi = 180°$,

$$\vec{E}_{TOT} = 2E_0 e^{-jkz}\hat{y} \qquad (32)$$

which is a vertically polarized wave.

In order to generate a horizontally polarized wave, the phase of the front spiral's excitation signal was delayed by an amount proportional to the wavelength of operation and the separation between the two planar antennas. The relationship between the phase delays (ϕ), wavelength (λ) and separation (d) is given by

$$\phi = \frac{2\pi d}{\lambda} \text{ rad.} \qquad (33)$$

For a frequency of operation of 1.2 GHz and separation of 10 mm, the required phase delays to be applied to the front planar antenna in order to achieve a horizontally polarized wave would be $-14.4°$. Figure 44 shows the amount of phase delay required for the same antenna separation operating at different frequencies.

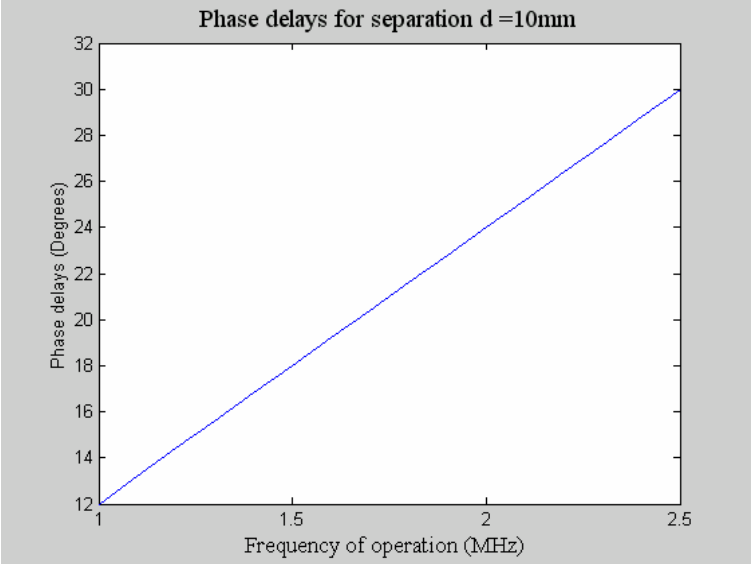

Figure 44. Phase delays required for an antenna separation of 10 mm.

The polarization of the fields at the antenna axis was verified through simulation. Figure 45 shows the vector plot of the resultant *E*-field components on the antenna plane at a distance of about 19.3 mm away from the antenna. Figures 46 to 48 show the individual *E*-field components in the *x*, *y* and *z*-directions. The antenna was found to be linearly polarized near the antenna axis. For the same delay settings, the polarization orientation was verified at a frequency of 2.4 GHz. Figures 49 to 52 show the *E*-field plots at that frequency with the front planar antenna delayed by $\phi = -14.4°$. The polarization of the antenna was also found to be linear at a frequency of 2.4 GHz. The far-field axial ratio plots for frequencies from 1.9 to 2.4 GHz are shown in Figures 53 to 58.

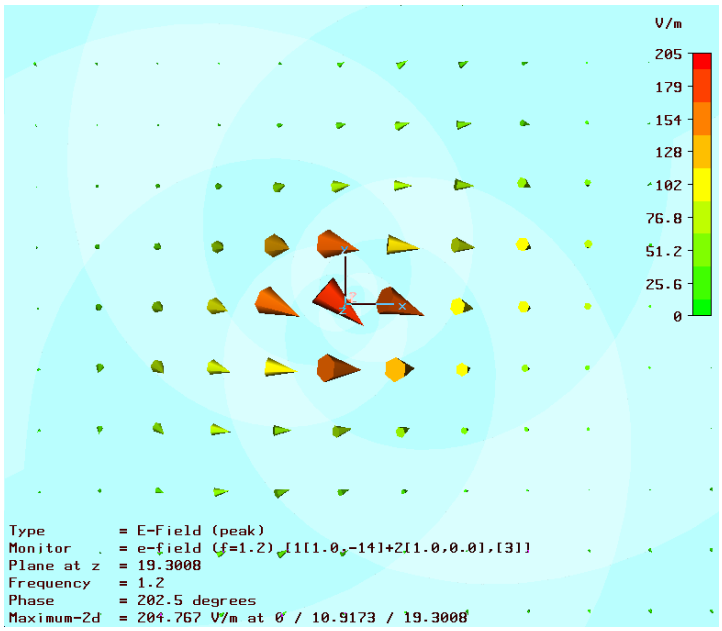

Figure 45. Vector plot of the resultant *E*-fields at frequency f=1.2 GHz.

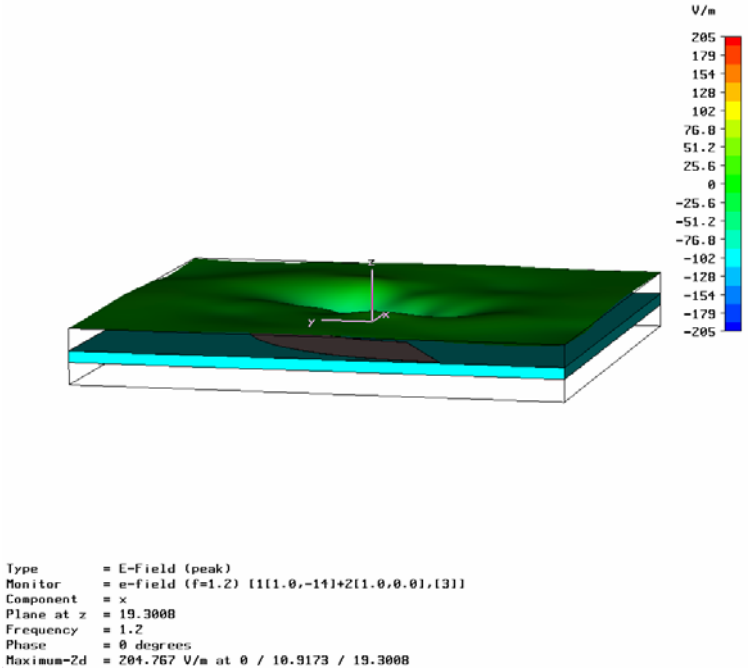

Figure 46. *E*-field component in the *x*-direction at frequency f=1.2 GHz.

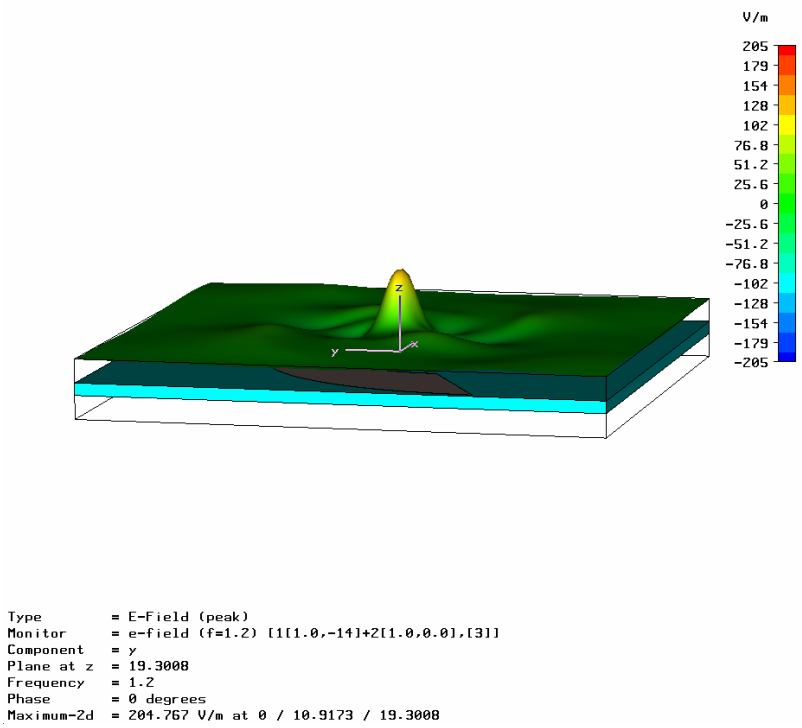

Figure 47. *E*-field component in the *y*-direction at frequency f =1.2 GHz.

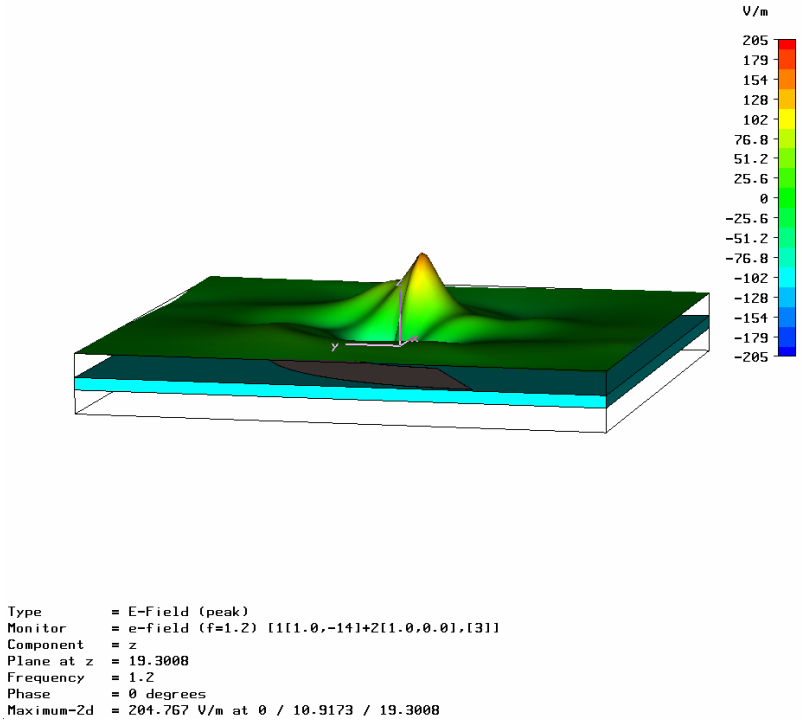

Figure 48. *E*-field component in the *z*-direction at frequency f =1.2 GHz.

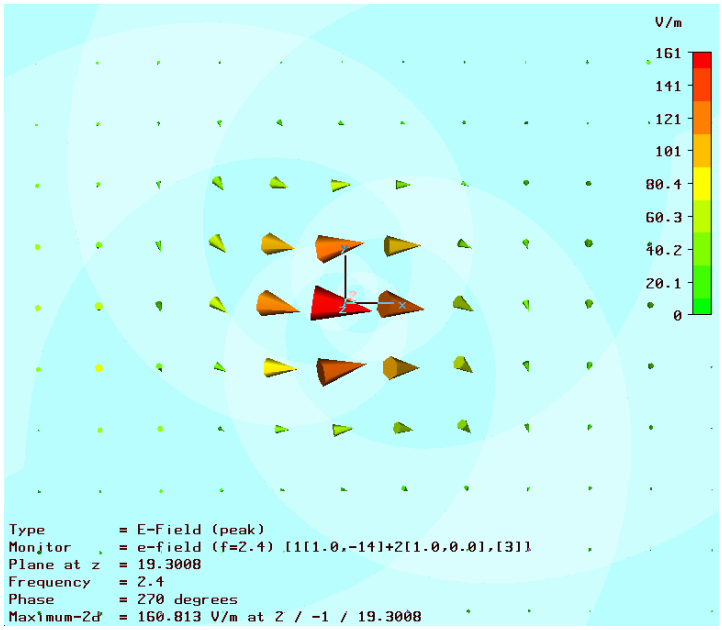

Figure 49. Vector plot of the resultant *E*-fields at frequency $f = 2.4$ GHz.

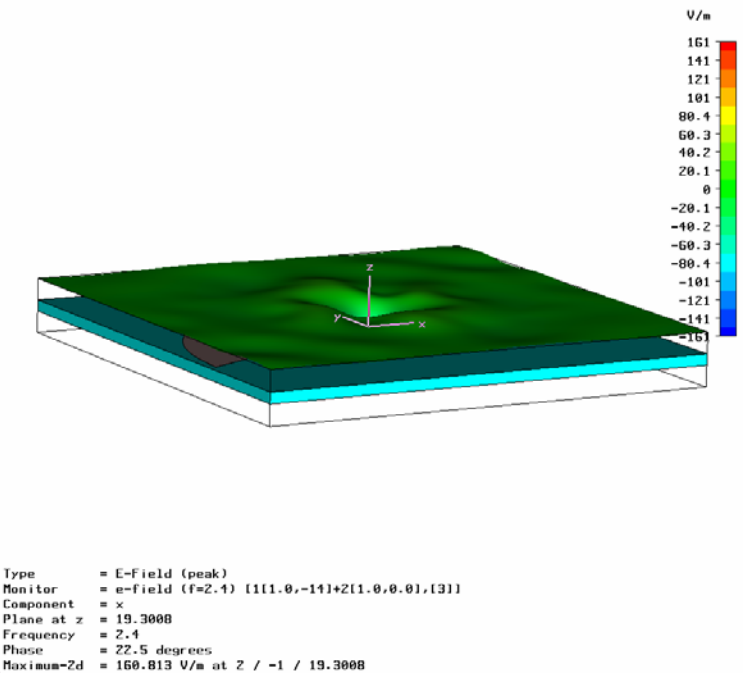

Figure 50. *E*-field component in the *x*-direction at frequency $f = 2.4$ GHz.

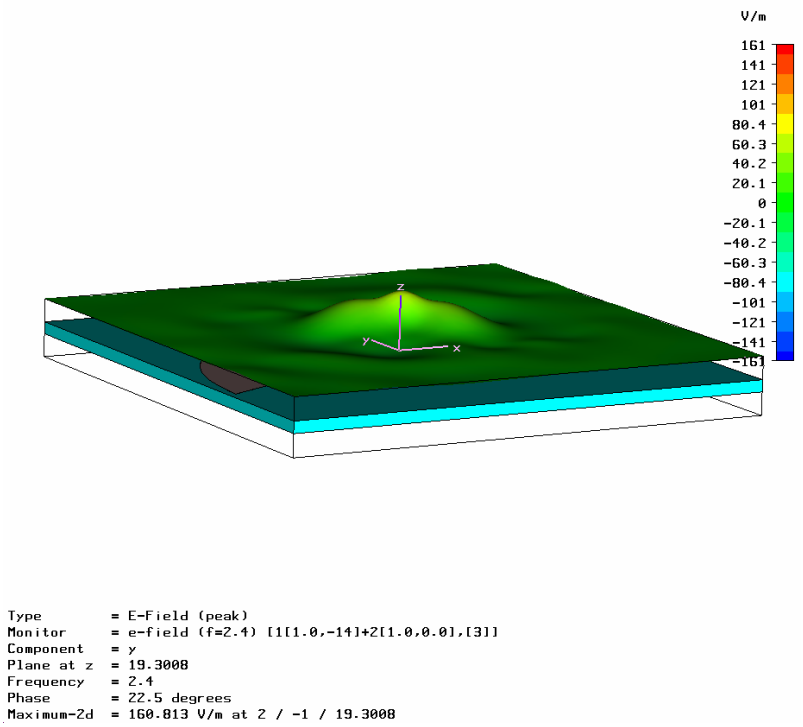

Figure 51. *E*-field component in the *y*-direction at frequency $f = 2.4$ GHz.

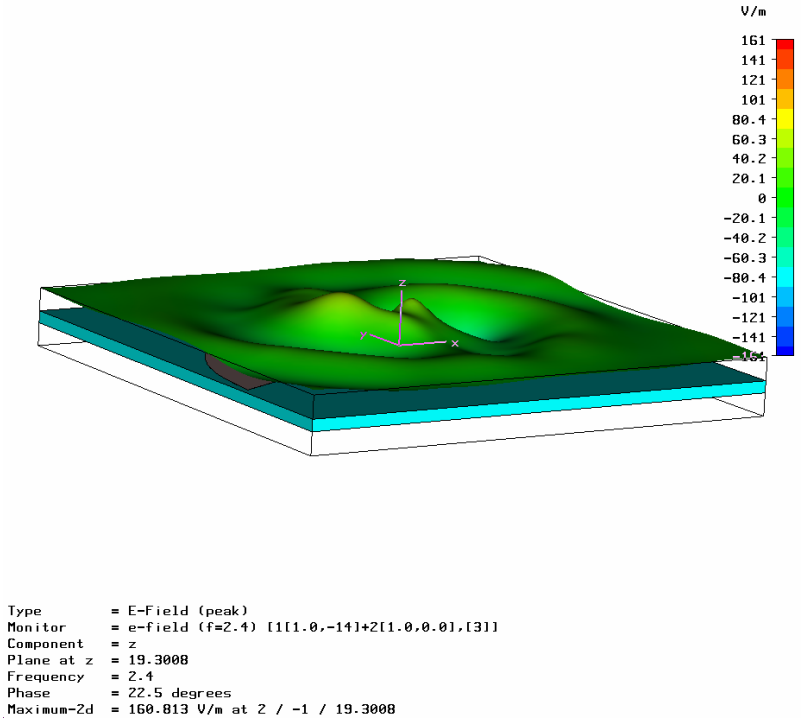

Figure 52. *E*-field component in the *z*-direction at frequency $f = 2.4$ GHz.

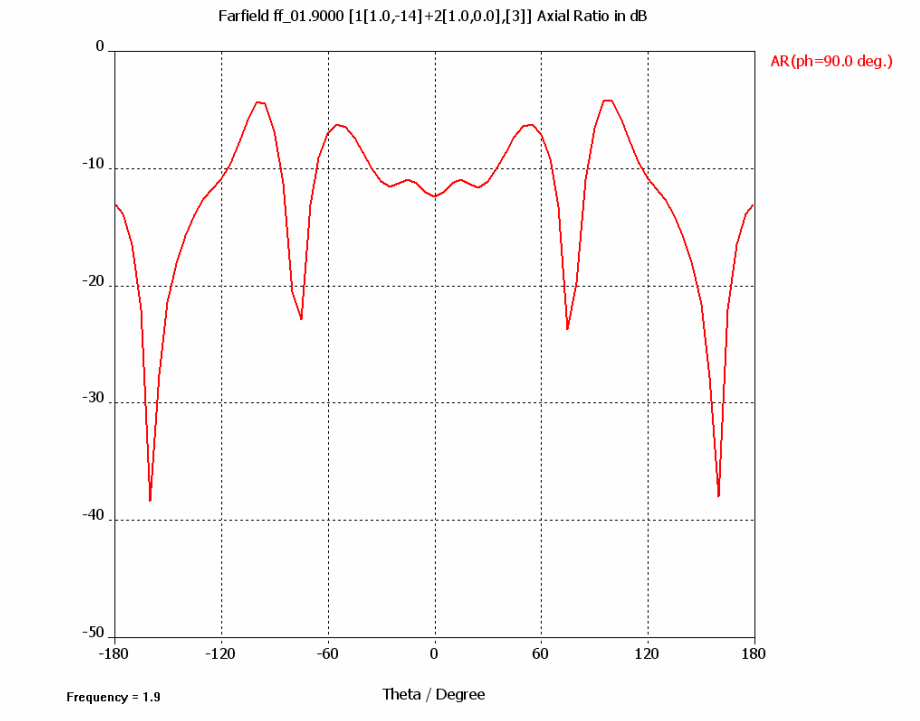

Figure 53. Axial ratio of the antenna at frequency $f = 1.9$ GHz.

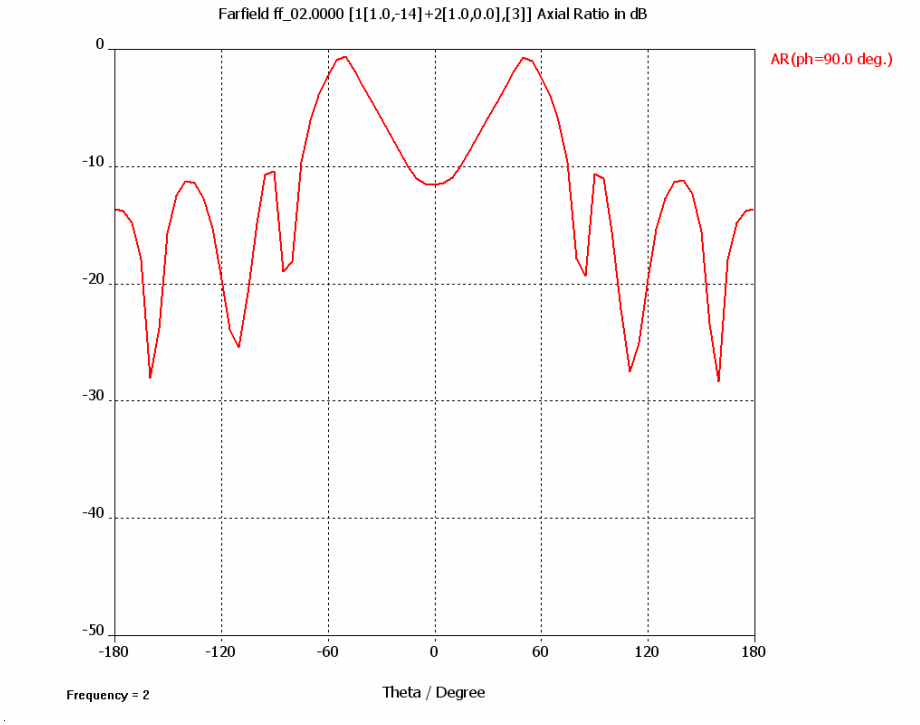

Figure 54. Axial ratio of the antenna at frequency $f = 2$ GHz.

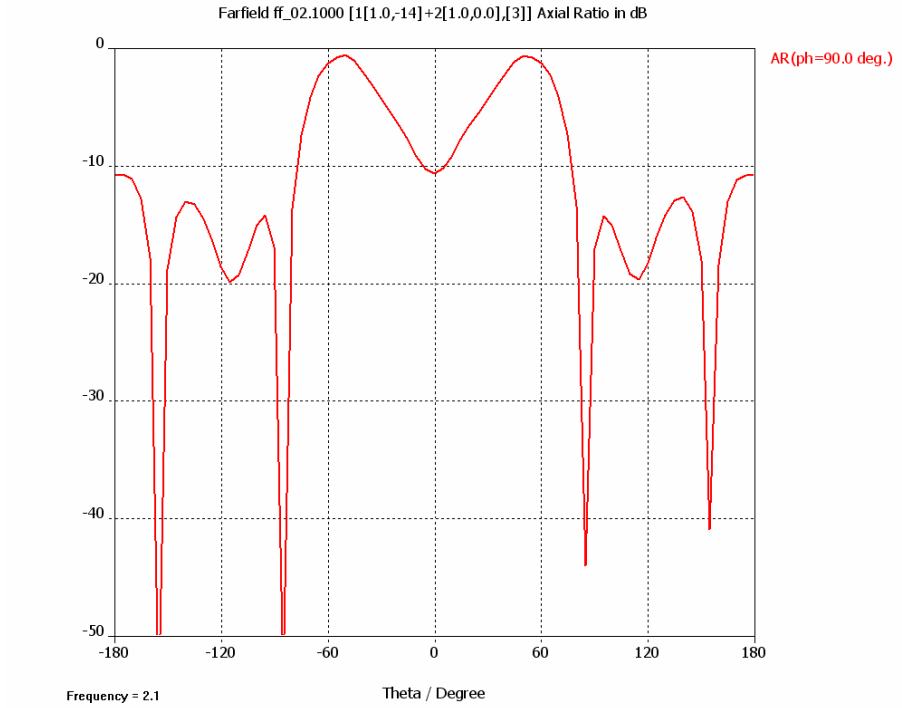

Figure 55. Axial ratio of the antenna at frequency f = 2.1 GHz.

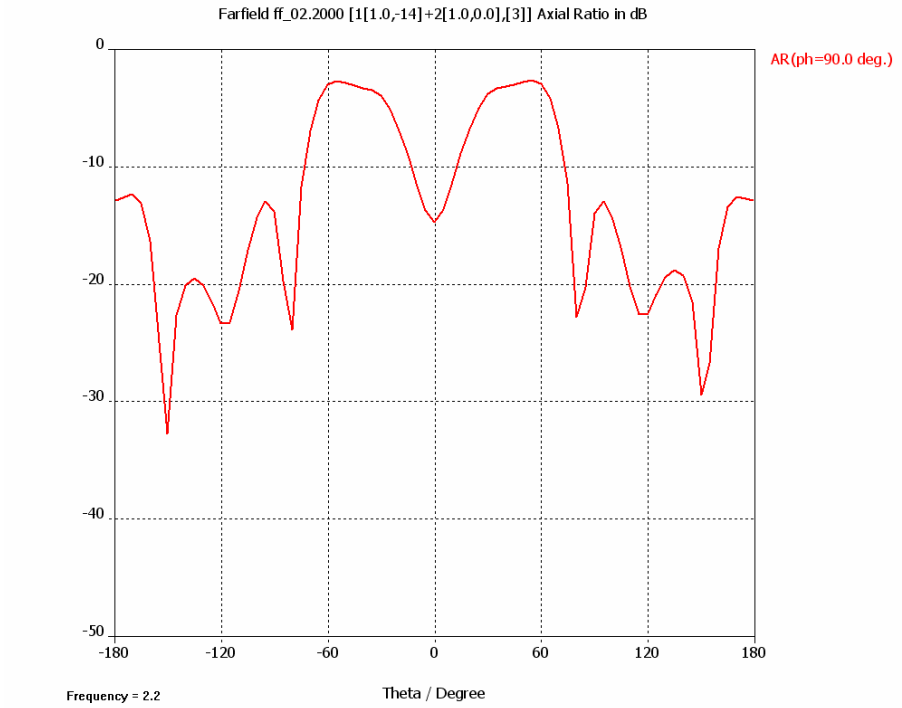

Figure 56. Axial ratio of the antenna at frequency f = 2.2 GHz.

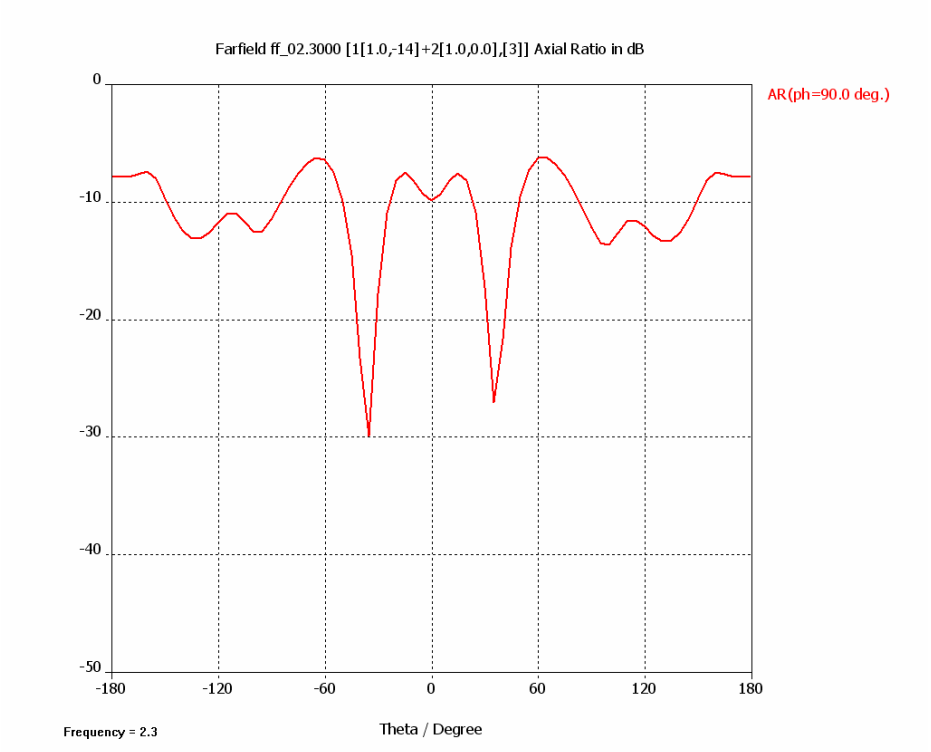

Figure 57. Axial ratio of the antenna at frequency f = 2.3 GHz.

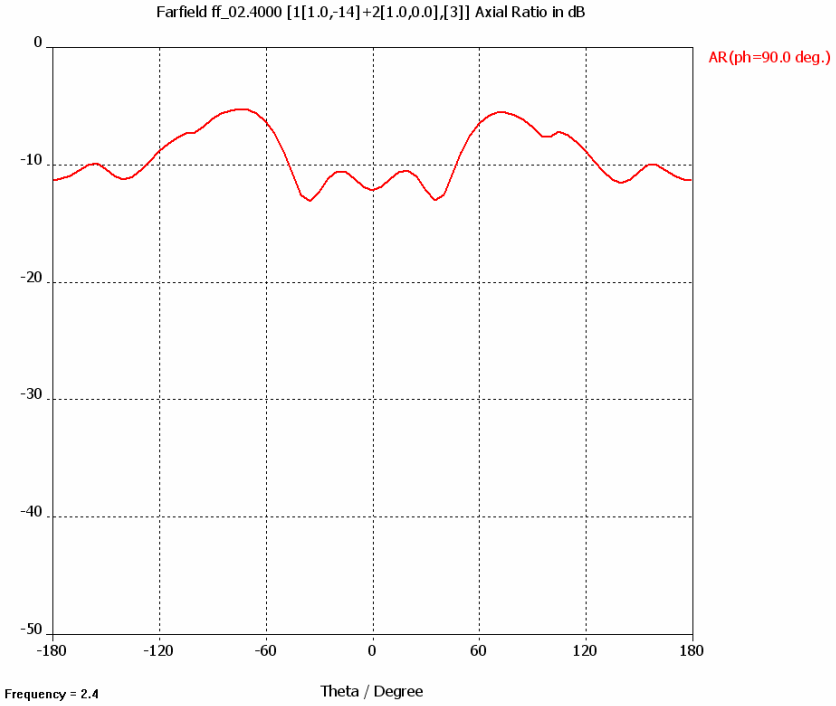

Figure 58. Axial ratio of the antenna at frequency f = 2.4 GHz.

As described previously, the polarization can be changed from a vertically polarized wave to a horizontally polarized wave by adding an additional phase delay of 180° degrees to the front spiral of the CWSA. A simulation was performed by changing the phase delays of the front planar antenna to $-104°$. The *E*-field components are shown in Figures 59 to 62. The $90°$ phase shift rotated the plane of polarization by $90°$ as expected.

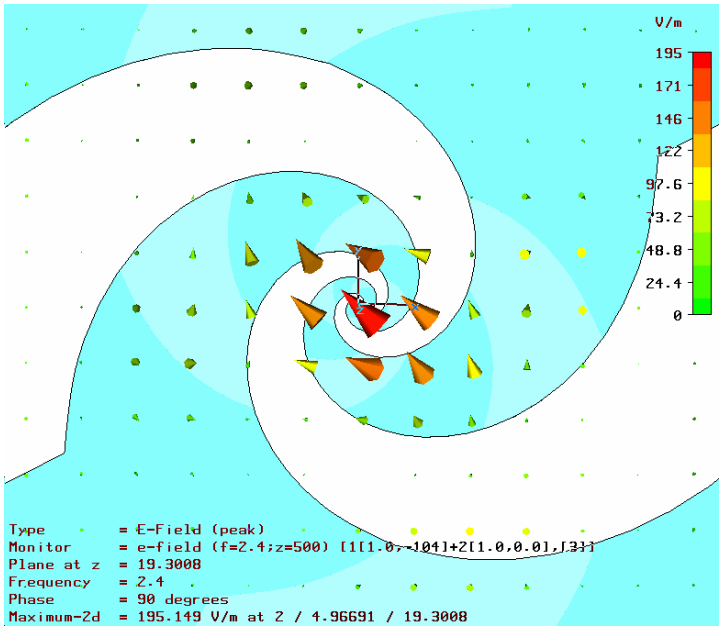

Figure 59. Vector plot of E-fields at frequency of 2.4 GHz with delay of $-104°$.

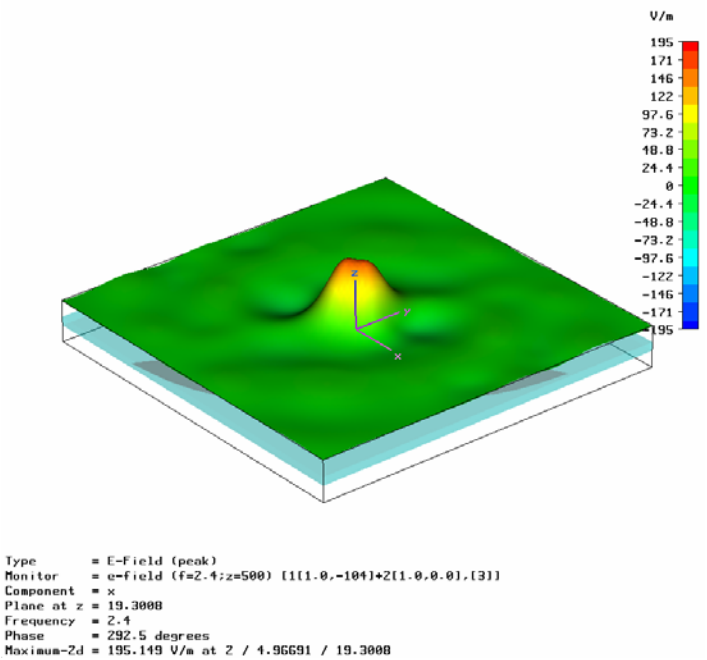

Figure 60. *E*-field component in the *x*-direction at frequency of 2.4 GHz with −104° delay.

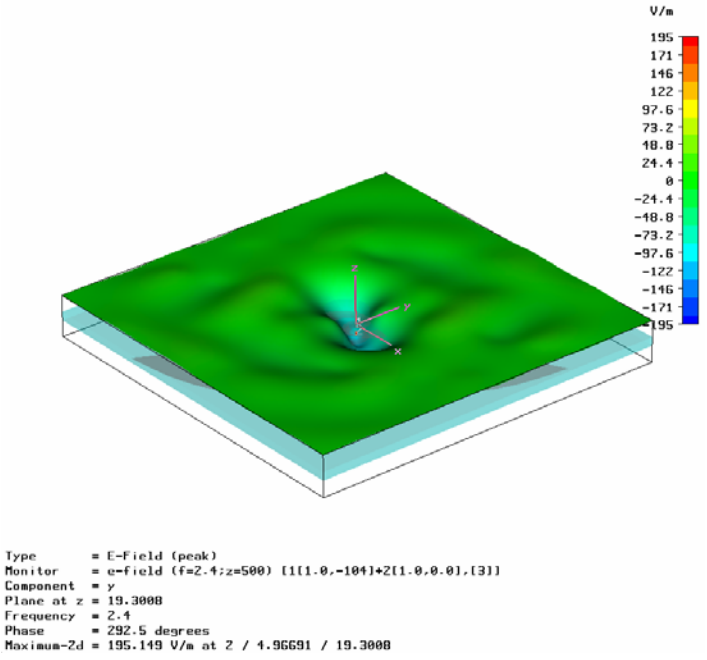

Figure 61. *E*-field component in the *y*-direction at frequency of 2.4 GHz with −104° delay.

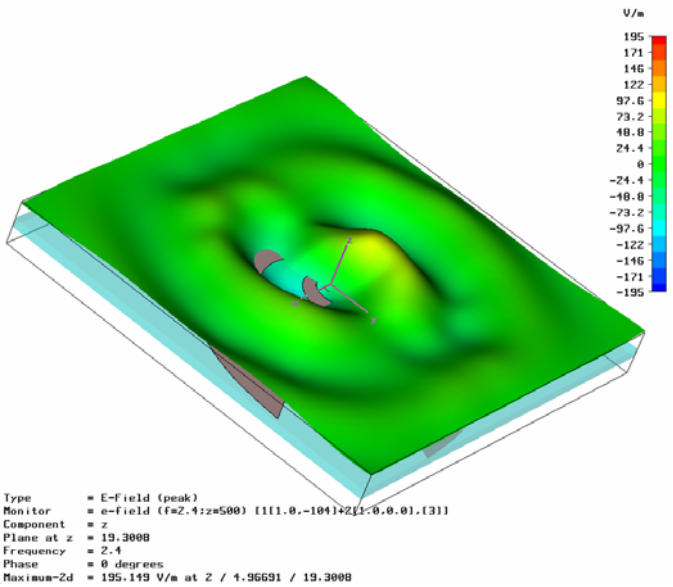

Figure 62. *E*-field component in the *z*-direction at frequency of 2.4 GHz with −104° delay.

B. SUMMARY

Several important aspects of the performance of the CWSA have been verified through a series of simulations. It has been shown that the rotated CWSA (with the plane of the front and rear spiral antenna planes rotated 90° to each other along the main antenna axis) gives a better performance in terms of reflections as compared to the unrotated case. The CWSA far-field polarization has also been verified to be linearly polarized on axis for any amount of delay applied to the input of the front planar antenna. The tilt angle of the linearly polarized wave can be changed from vertically polarized to a horizontally polarized by increasing the signal excitation delay to the front antenna by 180°. This allows buried objects with unknown aspect angle with respect to the receiving antenna to be detected and identified by the radar system without large polarization loss.

Use of the CWSA can be extended to other applications where a large antenna bandwidth is required. The CWSA retains the wideband antenna characteristics of the spiral antennas with an improved detection capability by using linearly polarized (both vertical and horizontal) waves.

V. CONCLUSIONS AND FUTURE WORK

A. CONCLUSIONS

This thesis has addressed many issues pertaining to the design of subsurface radar systems and wideband antenna design. In particular, the research investigated the factors contributing to the performance of a subsurface radar system, its architecture, and design of frequency-independent antennas. The result is a new antenna design, the counter-wound planar spiral, which is capable of variable linear polarization over a wide bandwidth.

Frequency-independent antennas refer to antennas that have no theoretical limitation on the bandwidth of operation. In practice, they are antennas whose radiation pattern, impedance, and polarization that remain virtually unchanged over a large bandwidth. A spiral antenna offers the advantages of having a large operating bandwidth, constant real impedance and a circularly polarized wave, which automatically reduces the amount of reflection received from the air/ground interface due to cross-polarization. The signal reception is, however, constrained by the target orientation with respect to the antenna axis. Only the co-polarized portion of the reflected wave from the object will be received by the antenna, which may result in 3-dB (6-dB for both transmit and receive) polarization loss, which is not acceptable in many applications.

This thesis examined the design and performance of a counter-wound spiral antenna. The CWSA can produce a linearly polarized wave in the forward direction by varying the phase of the excitation to the front planar spiral arms. The phase delay is dependent on the separation between the planar spiral arms and the frequency of operation. The resultant wave from the antenna will be linearly polarized. The plane of polarization can be made either horizontal or vertical by varying the delay to the antenna feeds. This design allows buried objects with unknown aspect angle with respect to the receiving antenna to be detected by the radar system without large polarization loss. Variable linear polarization allows the extraction of the maximum amount of information from the scattered echo. The reflections due to the returns from the air/ground interface can be reduced

by using signal processing techniques. The CWSA design may be extended to other applications where large antenna bandwidth is required.

B. FUTURE WORK

The counter-wound spiral antenna can be fabricated on a substrate, with its performance measured in the anechoic chamber. The antenna patterns of the fabricated antenna can then be measured and compared with the theoretical values and simulation results. The impedance match between the antenna feeds and the spiral antenna could be measured with test equipment and its effect on the overall antenna performance determined through measurements. However, it will be necessary to design a broadband balun.

For the model discussed here, the air/ground interface was a smooth, planar surface. In practical applications, the interface could be rough and may even support various forms of vegetation. The effects of these factors on the performance of the monostatic GPR using CWSA can then be determined by measurement. The benefits of using this antenna structure for bistatic GPR have not been examined and is worthy of investigation.

LIST OF REFERENCES

[1] Lacko, P.R., Clark W.W., Sherbondy, K., Ralston, J.M. and Dieguez, E., "Studies of ground-penetrating radar antennas," *2nd International Workshop on Advanced GPR*, pp. 24-29, 2003.

[2] Leimbach, G., Lowy, H., German Patent. No. 237944, 1910.

[3] Hűlsenbeck & Co., German Patent. No. 489434, 1926.

[4] Daniels, D.J., Gunon, D.J. and Scott, H.F., "Introduction to subsurface radar," *IEEE Proceedings F on Radar, Sonar and Navigation*, vol. 135, no. 4, pp. 278-320, 1988.

[5] Nilsson, B., "Two topics in electromagnetic radiation field prospecting," Doctoral Thesis, University of Lulea, Sweden, 1978.

[6] Olhoeft, G.R., "Applications and frustrations in using ground-penetrating radar," *IEEE Transactions on Aerospace and Electronic Systems Magazine*, vol. 17, no. 2, pp. 12-20, 2002.

[7] Jenn, D., "Ground Penetrating Radar," lecture notes on Radar system, Naval Postgraduate School, 2003.

[8] King, R.W.P. and Smith, G.S., *Antennas in Matter*, MIT Press, 1981.

[9] Pottel, R., *Dielectric Properties*, Plenum Press, 1973.

[10] Vant, M.R., Ramseier, R.O. and Makios, V., "The complex-dielectric constant of sea-ice at frequencies in range 0-1 to 40 GHz," *Journal of Applied Physics*, vol. 49(3), pp. 1264-1280, 1978.

[11] Larry, D.W., John, G.G, David, E.S. and Richard, V.B., "Surface snow properties effects on millimeter-wave backscatter," *IEEE Transactions on Geoscience and Remote Sensing*, vol. 26, no. 3, pp. 300-306, 1985.

[12] Georgi, S.B. and Sergei, D.K., "Loss-factor behavior of freshwater ice at 13.5 and 37.5 GHz," *IEEE Transactions on Geoscience and Remote Sensing*, vol. 36, no. 2, pp. 678-680, 1998.

[13] Parkhomenko, E.I., *Electrical Properties of Rocks*, Plenum Press, 1967.

[14] Keller, G.V., *Electrical Characteristics of the Earth's Crust*, Golem Press, 1971.

[15] Ulaby, F.T., Bengal, T., East, J. and Dobson, M.C., "Microwave properties of rocks," *IEEE Transactions on Geoscience and Remote Sensing*, vol. 3, pp. 1585, 1988.

[16] Zhang, Y.P., Zheng, G.X. and Sheng, J.H., "Radio propagation at 900 MHz in underground coal mines," *IEEE Transactions on Antennas and Propagation*, vol. 49, no. 5, pp. 757-762, 2001.

[17] Unterberger, R.R., "Radar propagation in rock salt," *Geophysical Prospecting*, vol. 26, no. 2, pp. 312-328, 1978.

[18] Dmitriev, W.V., Lobova, G.N. and Sukhov, V.I., "Dielectric properties of sand in range 0.4–13 MHz," *IEEE Transactions on Geoscience and Remote Sensing*, vol. 1, pp. 6-8, 1995.

[19] Fano, W.G. and Trainotti, V., "Dielectric properties of soils," 2001 *Conference on Electrical Insulation and Dielectric Phenomena*, pp. 75-78, 2001.

[20] John, O.C., "Moisture effects on the dielectric properties of soils," *IEEE Transactions on Geoscience and Remote Sensing*, vol. 39, no. 1, pp. 125-128, 2001.

[21] Neil, R.P., Fawwaz, T.U. and Myron, C.D., "Dielectric properties of soils in the 0.3-1.3 GHz," *IEEE Transactions on Geoscience and Remote Sensing*, vol. 33, no. 3, pp. 803-807, 1995.

[22] Tikkhonov, V.V., "Model of complex dielectric constant of wet and frozen soil in the 1-40 GHz frequency range," *IEEE Transactions on Geoscience and Remote Sensing*, vol. 3, pp. 1576-1578, 1994.

[23] Freundorfer, A., Lizuka, K. and Ramseier, R., "A method of determining electrical properties of geographical media," *Journal of Applied Physics*, vol. 55, no. 1, pp. 218-222, 1984.

[24] Takashi Iwasaki and Freundor, A., "A unidirectional semi-circle spiral antenna for subsurface radars," *IEEE Transactions on EMC*, vol. 36, no. 1, 1994.

[25] Dyson, J.D. and Mayes, P.E., "A note on the difference between equiangular and archimedes spiral antennas," *IRE Transactions on Microwave Theory and Techniques*, vol. 9, pp. 203-205, 1961.

[26] Hertel, T.H. and Smith, G.S., "The conical spiral antenna over the ground," *IEEE Transactions on Antennas and Propagations*, vol. 50, no. 12, 2002.

[27] Rumsey, V.H., *Frequency-Independent Antennas*, Electrical Science Series, Academic Press, 1966.

[28] Mayes, P.E., "Frequency-independent antennas and broad-band derivatives thereof," *Proceedings of IEEE*, vol. 80, pp. 103-112, 1992.

[29] Dyson, J., "The equiangular spiral antenna," *IEEE Transactions on Antennas and Propagation*, vol. 7, no. 2, pp. 181-187, 1959.

[30] Rumsey, V.H., Cheo, B.R.S. and Welch, W.J. "A solution to frequency-independent antenna problem," *IEEE Transactions on Antennas and Propagation*, vol. 9, no. 6, pp. 527-534, 1961.

[31] Pozar, D.M., *Microwave Engineering*, John Wiley & Sons, 2nd Ed., 1998.

[32] Deschamps, G., "Impedance properties of complementary multiterminal planar structures," *IEEE Transactions on Antennas and Propagation*, vol. 7, pp. 371-378, 1959.

[33] Thaysen, J., "A logarithmic spiral antenna for 0.4 to 3.8 GHz," *Applied Microwave & Wireless*, pp. 32-45, Feb 2001.

[34] Morgan, T., "Spiral antennas for ESM," *Antennas and Propagation Society International Symposium*, vol. 24, pp. 777-780, 1986.

[35] Thaysen, J., "Logarithmic spiral antenna and feed network for application to humanitarian de-mining," Department of Applied Electronics, Master Thesis, Technical University of Denmark, March 2000.

[36] Li, M.-Y., Tilley, K., Mccleary, J. and Chang, K., "Broadband coplanar strip-fed spiral antenna," *Electronics Letters*, vol. 31, pp. 176-177, 1994.

[37] Constantine A. Balanis, *Antenna Theory Analysis and Design*, John Wiley and Sons, 1982.

[38] Thaysen, J., "Characterization and optimization of a coplanar waveguide fed logarithmic spiral antenna," *IEEE AP-S Conference on Antennas and Propagation for Wireless Communication*, pp. 25-28, 2000.

[39] Jenn, D., *Radar and Laser Cross Section Engineering*, AIAA, 1995.

[40] Jenn, D., "Plane wave, transmission lines and waveguide," lecture notes on Radio Wave Propagation, Naval Postgraduate School, 2003.

[41] Peter R.L., William W.C. and Kelly S., "Studies of ground penetrating radar antennas," *2nd International Workshop on Advanced GPR*, pp. 24-29, 2003.

INITIAL DISTRIBUTION LIST

1. Defense Technical Information Center
   Ft. Belvoir, Virginia

2. Dudley Knox Library
   Naval Postgraduate School
   Monterey, California

3. John P. Powers, Chairman, Code EC
   Department of Electrical and Computing Engineering
   Naval Postgraduate School
   Monterey, California

4. Professor David Jenn, Code EC/Jn
   Department of Electrical and Computing Engineering
   Naval Postgraduate School
   Monterey, California

5. Professor Jeffrey Knorr, Code EC/Ko
   Department of Electrical and Computing Engineering
   Naval Postgraduate School
   Monterey, California

6. W.T. Wollny
   Quick Reaction Corporation
   Pebble Beach, California

7. Professor Yeo Tat Soon
   Director, Temasek Defence Systems Institute
   Singapore

7. Lim Teck Yong
   DSO National Laboratories
   Singapore